이학박사학위논문

Target-specific near-IR induced drug release and photothermal therapy with accumulated Au/Ag hollow nanoshells on pulmonary cancer cell membranes

금/은 빈 공간 나노쉘의 폐암 세포 표면 축적을 이용한 특정 세포 탐지 기능성 근적외선 유도약물 방출 및 광열 치료 효과

2015 년 8 월

서울대학교 융합과학기술대학원

융합과학부 나노융합전공

노 미 숙

A Dissertation for the Degree of Doctor of Philosophy

Target-specific near-IR induced drug release and photothermal therapy with accumulated Au/Ag hollow nanoshells on pulmonary cancer cell membranes

금/은 빈 공간 나노쉘의 폐암 세포 표면 축적을 이용한 특정 세포 탐지 기능성 근적외선 유도약물 방출 및 광열 치료 효과

August, 2015

By

Mi Suk Noh

Program in Nano Science and Technology

Graduate School of Convergence Science and Technology

Seoul National University

Target-specific near-IR induced drug release and photothermal therapy with accumulated Au/Ag hollow nanoshells on pulmonary cancer cell membranes

금/은 빈 공간 나노쉘의 폐암 세포 표면 축적을 이용한
특정 세포 탐지 기능성 근적외선 유도약물 방출 및 광열 치료 효과

By Mi Suk Noh

Supervised by Professor Myung-Haing Cho, D.V.M., Ph.D.

A Dissertation Submitted to the Faculty of the Graduated School of Seoul National

University in Partial Fulfillment of the Requirements for the Degree of Doctor of

Philosophy in Program in Nano Science and Technology

August 2015

Supervisory Committee Approval of Thesis submitted by

June 2015

Chairman :   Yoon-Kyu Song, Ph.D.   (signature)

Vice-Chairman: Myung-Haing Cho, D.V.M.,Ph.D. (signature)

Member :   Yoon-Sik Lee, Ph.D.   (signature)

Member :   Yuanzhe Piao, Ph.D.   (signature)

Member :   Bong-Hyun Jun, Ph.D.   (signature)

Abstract

Target-specific near-IR induced drug release and photothermal therapy with accumulated Au/Ag hollow nanoshells on pulmonary cancer cell membranes

(Supervisor: Myung-Haing Cho, D.V.M., Ph.D.)

Mi Suk Noh

Program in Nano Science and Technology,

Graduate School of Convergence Science and Technology

Seoul National University

Au/Ag hollow nanoshells (AuHNSs) were developed as multifunctional therapeutic agents for effective, targeted, photothermally induced drug delivery under near-infrared (NIR) light. AuHNSs were synthesized by galvanic replacement reaction. We further conjugated antibodies against the epidermal growth factor receptor (EGFR) to the PEGylated AuHNS, followed by loading with the antitumor drug doxorubicin (AuHNS-

EGFR-DOX) for lung cancer treatment. AuHNSs showed similar photothermal efficiency to gold nanorods under optimized NIR laser power. The targeting of AuHNS-EGFR-DOX was confirmed by light-scattering images of A549 cells, and doxorubicin release from the AuHNSs was evaluated under low pH and NIR-irradiated conditions. Multifunctional AuHNS-EGFR-DOX induced photothermal ablation of the targeted lung cancer cells and rapid doxorubicin release following irradiation with a NIR laser. Furthermore, we evaluated the effectiveness of AuHNS-EGFR-DOX drug delivery by comparing two drug delivery methods: receptor-mediated endocytosis and cell-surface targeting. Accumulation of the NPs on the cell surfaces by targeting EGFR demonstrated more effective for lung cancer treatments than uptake of AuHNS-EGFR-DOX. Taken together, our data suggest a new and optimal method of NIR-induced drug release, via the accumulation of targeted AuHNS-EGFR-DOX on cancer cell membranes.

Student Number: 2009-31184

Table of Contents

List of Figures

List of Schemes

List of Abbreviation

A549   adenocarcinomic human alveolar basal epithelial cells

AgNS   silver nanoshell

AuHNS-EGFR-DOX EGFR antibody-conjugated and doxorubicin-loaded AuHNS

AuHNSs   Au/Ag hollow nanoshells

CA   calcein AM

CLSM   confocal laser scanning microscopy

CTAB   cetyltrimethylammonium bromide

DI   deionized

DMSO   dimethylsulfoxide

EDC   N-(3-dimethylaminopropyl)-N'-ethylcarbodiimide hydrochloride

EDX   energy dispersive X-ray spectroscopy

EF-TEM   energy-Filtering Transmission Electron Microscope

EG   ethylene glycol

EGFR   epidermal growth factor receptor

Eth-1   ethyl homodimer-1

FBS   fetal bovine serum

FIB	focused ion beam
GNRs	Au nanorods
H522	non-small lung cancer cells
$HAuCl_4$	tetrachloroaurate trihydrate
HNSs	hollow nanoshells
HOOC-PEG-SH	poly(ethylene glycol)-2-mercaptoethyl ether acetic acid
HRP	horseradish peroxide
HSs	hollow-shells
MDR	multi-drug resistance cells
mPEG-SH	methoxy poly(ethylene glycol) sulfhydryl
MPTS	3-mercaptopropyl trimethoxysilane
MTT	3-(4,5-dimethylthiazo-2-yl)2, 5-diphenyltetrazolium bromide
NHS	N-hydroxysuccinimide
NIR	near-infrared
NP	nanoparticle
NS	nanoshell
OA	octylamine
PBS	phosphate-buffered saline

PTT	photothermal therapy
PVP	polyvinylpyrrolidone-40
QDs	quantum dots
SDS-PAGE	sodium dodecylsulfate-polyacrylamide gel electrophoresis
SEM	scanning electron microscope
SPR	surface plasmon resonance
TEM	transmission electron microscopy
TEOS	tetraethyl orthosilicate

Target-specific near-IR induced drug release and photothermal therapy with accumulated Au/Ag hollow nanoshells on pulmonary cancer cell membranes

Introduction

1. Nanosystem for biological application and drug delivery

The integration of multiple characteristics into monodisperse nanosystems has been a goal of biological research. Nano-sized vehicles with multifunctionality including diagnostic and therapeutic capabilities could provide synergistic advantages such as specific targeting, multimodal imaging, controlled release of drugs, and simultaneous diagnostics and therapy [1].

Drug-delivery systems with NPs show a clear potential for cancer treatments in view of advantages such as the ability to target specific locations by reducing the concentration of the drug at non-target sites, and high therapeutic efficiency of drug release [2]. Generally, conventional cancer treatments such as surgery, radiation, and chemotherapy has shown the limitations of selective therapy toward tumor cells, often giving rise to severe side effects in healthy tissues [2].
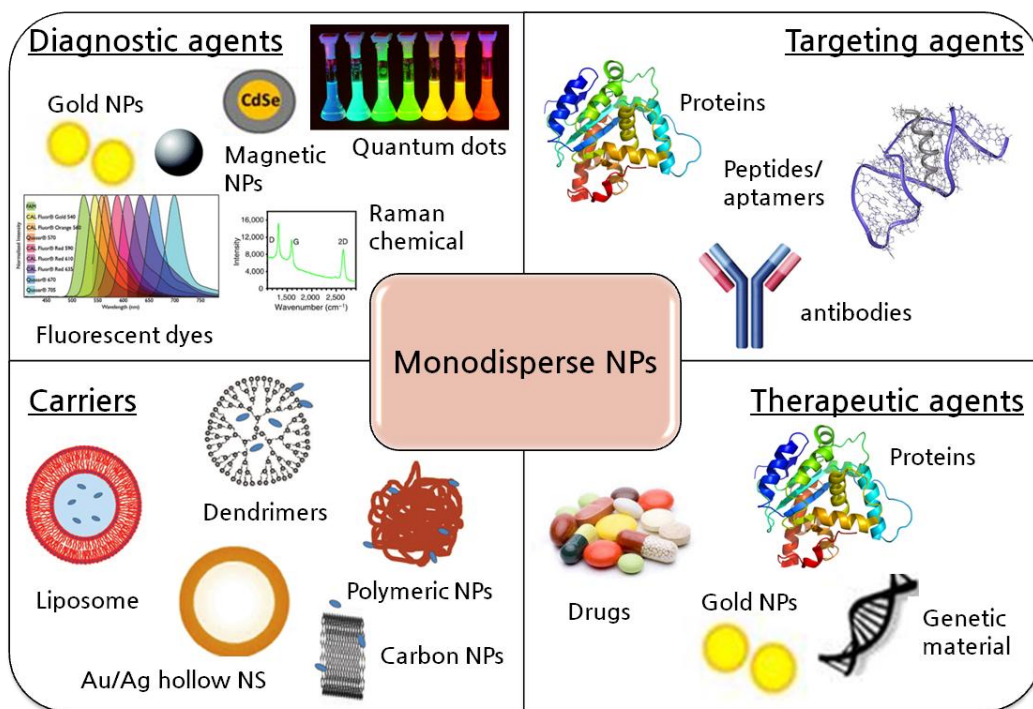
Figure I. **Monodisperse nanoparticles with diverse modifications for biological applications and drug delivery.**

2. Nanocarriers for drug delivery by photothermal therapy and chemo-thermo therapy

Effective drug delivery by nanocarriers has been intensively investigated using dendrimers [3, 4], polymeric micelles [5], liposomes [6, 7], carbon-based materials [8-10], magnetic particles [11, 12], and noble metal nanoparticles (NPs) [9, 13]. Nanocarriers were developed to protect drugs from premature degradation and to enhance drug absorption into specific tissues. Compared to organic carriers, which only serve as a drug reservoir, novel metal NPs have many advantages and are multifunctional, due to their unique optical properties and the various surface functional groups that can be introduced.

Near-infrared (NIR) resonant nanomaterials such as Au nanorods (GNRs) [9, 14, 15], multi-branched particles [16, 17], nanoshells [18], and hollow-shells (HSs) [13, 19] are attractive therapeutic agents because they can deliver drugs via non-invasive hyperthermia. NIR light in the range of 700–900 nm has been widely used to locally raise cell temperature, thereby optimizing the photothermal effect [20].

Triggered drug release by an external stimulus such as NIR irradiation could significantly advance cancer treatment by overcoming the indiscriminate drug distribution observed in conventional drug delivery. The combination of photothermal therapy (PTT)

and chemotherapy, termed chemo-thermotherapy [19], can achieve enhanced anticancer

efficacy via synergistic effects.
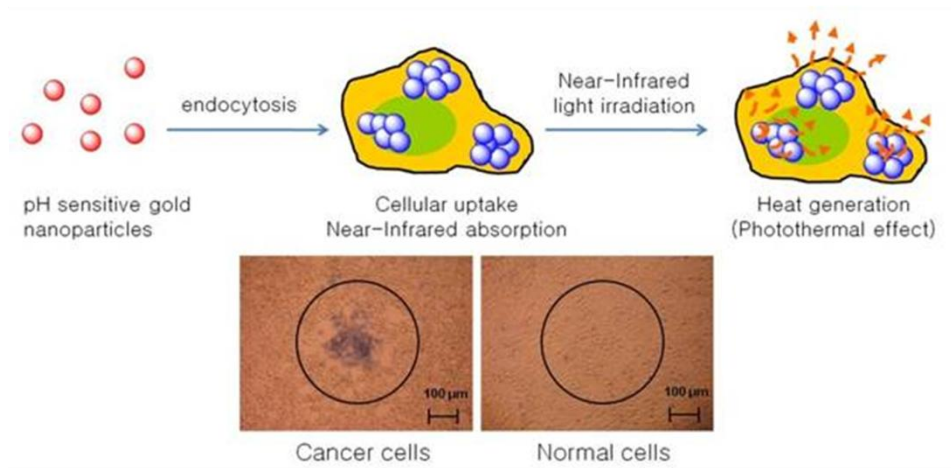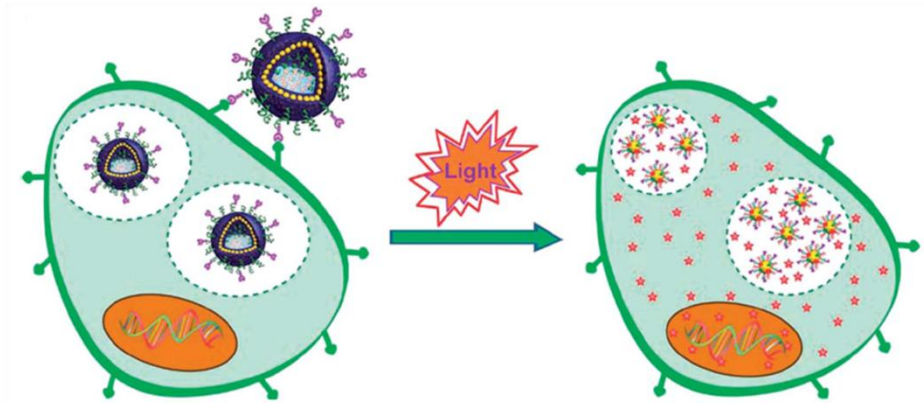
Figure II. **Nanocarriers for drug delivery by photothermal therapy and chemo-thermo therapy. A.** photothermal effects for cancer cells by gold nanoparticles (NPs) [21]. **B.** Triggered drug release with nanocarriers into the cell cytoplasm by NIR irradiation [22].

3. Research objective : Development of drug delivery methods with Au/Ag hollow nanoshell (AuHNS) by targeting cancer cells

Previous reports have shown that nanocarriers are internalized by cells through endocytosis; however, these nanocarriers were not specifically targeted to cancer cells [19, 23, 24]. Drug carriers that specifically target cancer cells are advantageous, because they selectively kill cancer cells with minimal side effects, particularly when combined with controlled drug release. Thus, we sought to develop novel drug-loaded nanocarriers that could reach the desired cancer cells or tissues via selective tumor cell targeting [25, 26].

We chose Au/Ag hollow nanoshell (AuHNS) to develop a novel, multifunctional nanocarrier for selective chemo-thermotherapy. The hollow nanoshells (HNSs) are advantageous for chemo-thermotherapy, because they are simply synthesized by galvanic replacement reactions from Ag nanoshells (NSs) [19, 27]. Furthermore, the hollow vacancy allows for high drug loading, due to the large effective surface areas for drug attachment [28]. In addition, in contrast to GNR, cytotoxic surfactants such as cetyltrimethylammonium bromide (CTAB) are not used during the preparation of HNS structures [19, 27, 29].

In this study, we report a novel, multifunctional therapeutic agent- doxorubicin-loaded, anti-EGFR antibody-conjugated and PEGylated Au/Ag nanoshells (AuHNS-EGFR-DOX)

which can selectively target cancer cells and kill them via photothermal-induced drug release. In this system, AuHNS emits a strong surface plasmon resonance (SPR) band in the NIR region for photothermal drug delivery, EGFR is a marker allowing for specific targeting of cancer cells [30-32], and doxorubicin is a chemotherapeutic agent [6, 19, 28, 33]. Targeting was confirmed by light-scattering images of lung cancer cells, and drug release was evaluated under low pH and NIR irradiation conditions.

Additionally, we developed a novel approach to maximize the ability of multifunctional NPs to kill lung cancer cells by evaluating two drug-delivery mechanisms: receptor-mediated endocytosis and the accumulation of targeted AuHNS-EGFR-DOX on the cell membranes. In previous reports, NIR irradiation-induced drug release was shown to be dependent on endocytosis [19, 23, 24, 34]. Our data suggest a new and optimal method of NIR-induced drug release, via the accumulation of targeted AuHNS-EGFR-DOX on cancer cell membranes.

Materials and Methods

1. Materials

Tetraethylorthosilicate (TEOS), 3-mercaptopropyl trimethoxysilane (MPTS), ethylene glycol (EG), poly(vinyl pyrrolidone) (PVP, Mw ~40,000), silver nitrate (AgNO$_3$, 99.99+ %), octylamine (OA), tetrachloroaurate trihydrate (HAuCl$_4$, 99.9+ %), doxorubicin, *N*-hydroxysuccinimide (NHS), and *N*-(3-dimethylaminopropyl)-*N'*-ethylcarbodiimide hydrochloride (EDC) were purchased from Sigma-Aldrich (St. Louis, MO, USA) and used without further purification. PEG coated GNR (GR750-PG-1mL) were purchased from Nanocos (New York, USA). Absolute ethanol (99.8 %) was purchased from Carlo Erba (Milano, Italy). Methoxypoly(ethylene glycol)sulfhydryl (m PEG-SH, Mw 5,000) was purchased from Sunbio (Anyang, Korea). Poly(ethylene glycol)-2-mercaptoethyl ether acetic acid (HOOC-PEG-SH, Mw 5,000) was purchased from Creative PEG Works (Winston Salem, NC, USA). Ammonium hydroxide (NH$_4$OH, 27 %), sodium chloride, and ethanol (98 %) were purchased from Daejung (Busan, Korea). Deionized (DI) water was used for all experiments.

2. Cell culture

A549 (adenocarcinomic human alveolar basal epithelial cells) and H522 cell lines (non-small lung cancer cells) were obtained from Korean cell line bank (Seoul, Korea). A549 cell line was grown in F-12 medium and H522 cell line was grown in RPMI-1640 medium. The media for A549 and H522 cell lines were supplemented with 10 % fetal bovine serum and 1 % penicillin/streptomycin (GibcoBRL, Grand Island, NY, USA). The cells were kept at 37 °C in a humidified atmosphere containing 5 % CO_2.

3. Preparation of Au/Ag hollow-nanoshells (AuHNSs)

Tetraethylorthosilicate (TEOS, 1.6 mL) was dissolved in 40 mL of absolute ethanol, followed by addition of a 3 mL portion of aqueous ammonium hydroxide (~27 %). The resulting mixture was vigorously stirred using a magnetic bar for 20 h at room temperature. The resulting silica NPs were centrifuged and washed with ethanol several times to remove the excess reagents. The resulting silica NPs were then functionalized with the thiol group. Silica NPs (300 mg) were dispersed in 6 mL of ethanol containing 300 μL of MPTS and 60 μL of aqueous ammonium hydroxide (27 %, v/v). The mixture was stirred for 12 h at room temperature, after which the MPTS-treated silica NPs were centrifuged and washed with ethanol several times. In order to synthesize Ag nanoshells (AgNS), 2 mg of MPTS-treated silica NPs were dispersed in 25 mL of ethylene glycol

containing PVP (5 mg), followed by the addition of a 25 mL of AgNO$_3$ solution in ethylene glycol (final concentration of AgNO$_3$ was 3.5 mM). Next, 41.3 μL of octylamine (5 mM) was rapidly added to the NP solution, which was stirred for 1 h at room temperature. The resulting AgNSs were centrifuged and washed with ethanol several times for purification. To form hollow structure *via* galvanic replacement reaction, 100 μL aliquot of AgNS (10 mg/mL) was dispersed in 5 ml of PVP (8 wt %, MW 40,000) aqueous solution. Next, 0.1 mM of HAuCl$_4$ solution was loaded into a plastic syringe with PVC tubing, and was placed on a syringe pump, which was used to add HAuCl$_4$ solution (4.5 mL, 0.1 mM) to the AgNS dispersion at a rate of 0.75 mL/min at 110 ℃. After adding the HAuCl$_4$ solution, the reaction was allowed to stabilize the Au/Ag hollow-nanoshells (AuHNSs) for 10 min, after which the dispersion was cooled to room temperature with vigorous magnetic stirring. The resulting mixture was washed with a saturated solution of NaCl to remove residual AgCl, centrifuged and washed with DI water (×3) and ethanol (×3). In order to confer biocompatibility and functionality, the AuHNS surface was grafted with two types of PEG derivative depending on the further modification. For conjugation with EGFR antibody, the AuHNS surface was modified with HOOC-PEG-SH solution (2 mM in ethanol). The PEG grafted AuHNS (AuHNS-COOH) dispersions were washed with ethanol several times by centrifugation and then resuspensed in 0.1 M of phosphate buffered saline (PBS, pH 7.0).

4. Preparation of AuHNS-EGFR antibody

After the activation of carboxylic acid group with 2 mM of EDC and 5 mM of NHS in 0.1 M of PBS (pH 6.0), 20 μg portion of the antibody (Santa Cruz Biotechnology, Santa Cruz, CA, USA) was added to the pre-activated PEGylated AuHNS dispersion. The mixture was shaken for 2 h at room temperature. The EGFR antibody conjugated AuHNSs were rinsed with 0.1 M of PBS (pH 7.0) several times.

5. Loading of doxorubicin on AuHNS

Doxorubicin was loaded into AuHNS or AuHNS-EGFR (1 mg/mL) by mixing the NPs with a doxorubicin solution (1 mg/mL) in PBS (pH 7.0, 0.1 M, 1 mL). The mixture was gently shaken at room temperature for 24 h in the dark. Free doxorubicin was removed by washing with PBS (pH 7.0) several times by centrifugation.

To determine the amount of doxorubicin loading, the calibration curve was obtained based on the absorbance at 480 nm using various concentrations of doxorubicin dissolved in 0.l M of PBS (pH 7.0). The amount of doxorubicin loading in NPs was then estimated by the absorbance of doxorubicin-loaded AuHNS or AuHNS-EGFR.

6. Characterization of AgNS and AuHNS

Energy-Filtering Transmission Electron Microscope (EF-TEM) images of AgNS and AuHNS were obtained using a LIBRA 120 (Carl Zeiss, Germany). UV-Vis-NIR spectra were collected with a UV-Vis-NIR spectrophotometer (Optizen 2120 UV, Mecasys Co. Ltd., Daejeon, South Korea). Cross-sectional scanning electron microscope (SEM) images of AgNS and AuHNS were obtained with dual beam focused ion beam (FIB) microscope (Helios 550 NanoLab DualBeam, FEI Corporate, Oregon, USA). Prior to obtain the imaging with SEM, a sample stage was tillted and the AgNS and AuHNS particles were milled with a Ga^+ ion beam.

7. Verification of photothermal properties of AuHNS

To verify the photothermal activity of NPs, 500 μL of PEGylated AuHNSs (1 mg/mL) in a glass vial was irradiated by 800 nm NIR laser with an intensity of 800 mW/cm^2 for 10 min, and the temperature change was measured by a digital thermometer.

To find the optimal laser power, the NIR laser was applied to A549 cells at a diverse range of power levels. The cells were incubated in a 6-well plate with confluency of 50,000 cells/well. After 1 day incubation, the wells were treated by NIR laser irradiation (31.3, 62.5, 125, 187.5, and 250 mW/cm^2, diameter 2 mm, 10 s). To visualize live and dead cell with two-color fluorescence, the Live/Dead viability/cytotoxicity kit (Invitrogen,

CA, USA) which contains ethyl homodimer-1 (eth-1) and calcein AM (CA) was used according to the manufacturer's protocol. Immediately after NIR laser irradiation, cells were washed once with PBS and incubated with 4 μM eth-1 and 2 μM CA for 30 min at room temperature. Fluorescence was assessed by confocal laser scanning microscopy (CLSM, Carl Zeiss, Germany).

To examine hyperthermia by photothermal effects, A549 cells (50,000 cells/well in a 6-well plate) were treated with PEGylated AuHNSs (3.0×10^{10}, 200 μL in PBS) and PEGylated GNRs (3.0×10^{10}, 200 μL in PBS) for 8 h in a humidified 5 % CO_2 incubator at 37 °C. Residual NPs were washed with PBS several times. The media in the wells were replaced with serum-containing media. A549 cells that took up AuHNSs were irradiated with 800 nm NIR laser with an intensity of 125 mW/cm^2 for 10 s. Immediately after irradiation, the cells were stained with trypan blue (Gibco, Grand Island, New York, USA) for 10 s and the images of stained cell were obtained with × 20 lens using an inverted microscope (eclipse TS100, Nikon, Japan).

8. Cytotoxicity assay

A549 cells were maintained at 37 °C, 5% CO_2 in F-12 medium containing 10 % fetal bovine serum (FBS) and 1 % penicillin/streptomycin with density of 5,000 cells/wells. After incubation for 8 h at 37 °C with diverse concentration ($0.8 - 3.0 \times 10^{10}$/mL, 100 μL)

of AuHNS and GNR, the cellular toxicity was evaluated using the 3-(4,5-dimethylthiazo-2-yl)-2,5-diphenyltetrazolium bromide (MTT) assay (Sigma-Aldrich). Briefly, 20 μL MTT solution (5 mg/mL) was added to the well and incubated with the cells for 4 h at 37 °C. The cells were treated with 100 μL of dimethylsulfoxide (DMSO, Sigma-Aldrich) and the absorbance was quantified at 570 nm using an ELISA reader (BioRad, Hercules, CA, USA).

9. HRP detection of AuHNS and AuHNS-EGFR

To confirm the conjugation of anti-EGFR on AuHNS-EGFR, nitrocellulose membranes were exposed to AuHNS and AuHNS-EGFR. Immunoblotting was performed in 5 % skim milk, and the membranes were exposed to secondary antibodies conjugated to horseradish peroxide (HRP) for 1 h at room temperature. After washing, the AuHNS and AuHNS-EGFR treated zone on nitrocellulose were visualized using an image analyzer ATTO (ATTO Corp., Tokyo, Japan).

10. Western blotting

After measuring the protein concentration of the lysates from A549 and H522 cell lines using a Bradford Protein Assay Kit (Bio-Rad), equal amounts (25 μg) of protein were separated by 10–15 % sodium dodecylsulfate-polyacrylamide gel electrophoresis (SDS-

PAGE) and transferred to nitrocellulose membranes. The membranes were blocked with TBST containing 5 % skim milk for 1 hour at room temperature and immunoblotting was performed by overnight incubation at 4 °C with the EGFR primary antibodies (Santa Cruz Biotechnology, Santa Cruz, CA, USA) in 5 % skim milk and the membranes were exposed to secondary antibodies conjugated to horseradish peroxide (HRP) for 1 h at room temperature. After washing, the bands-of-interest were visualized using by an image analyzer ATTO (ATTO Corp).

11. *Dark field imaging of EGFR conjugated AuHNS*

A549 and H522 cells were incubated in a Lab-tek glass chamber slide (Nalge Nunc, International, Rochester, NY, USA) with a density of 50,000 cells/well in a CO_2 incubator for 1 day. Then, the cells were fixed with paraformaldehyde (4 %) for 15-30 min at 25 °C. The cells were washed with 0.1 M of PBS (pH 7.0) three times to remove the fixing agent. The fixed cells were treated with AuHNS-EGFR or AuHNS-EGFR-DOX (3.0×10^{10}/mL, 100 μL) in PBS at 4 °C overnight for targeting. After targeting AuHNS-EGFR or AuHNS-EGFR-DOX, the residual NPs were removed by careful washing ($1\times$) with PBS solution for several times. When the slides were dried, the surfaces of the slides were covered with a cover slip and, the slides were observed with dark field microscope (Eclipse TE2000-S, Nikon, Tokyo, Japan).

12. Doxorubicin release from AuHNS

Doxorubicin release was measured at different pH levels and with or without NIR irradiation. To monitor the release of doxorubicin, AuHNS-DOX was dispersed in citrate buffer (pH 5.0) and PBS (pH 7.4) at room temperature. At designated time points, the solution of the NPs was centrifuged at 13,000 rpm for 5 min to pull down the NPs. To measure the amount of the released doxorubicin, the absorbance of supernatant was measured at 480 nm. Also, the effects of doxorubicin release by 800 nm laser irradiation were carried out for 30 s at 125 mW/cm^2. Then, the AuHNS-DOX solution in PBS was centrifuged at 3,000 rpm for 5 min, and the concentration of the released doxorubicin in the supernatant was determined by measuring the absorbance at 480 nm by UV spectrophotometer (OPTIZEN 2120UV, Mecasys, Daejeon, Korea) before and after laser irradiation. .

13. Cell viability assay of nanoparticles

A549 cells were exposed to AuHNS, AuHNS-EGFR, AuHNS-DOX, AuHNS-EGFR-DOX (3.0×10^{10}/mL, 100 μL) for 2 h at room temperature. A549 cells were also treated with free doxorubicin (0.5 μg/mL) for 2 h to compare drug release effects. After washing the cells, they were divided into two groups for NIR irradiation and without NIR irradiation. The intensity of NIR irradiation was 125 mW/cm^2 (diameter 2mm, 10 s).

A549 cells were exposed to radiation in 96-well plates at a density of 1×10^4 cells/well. After NIR irradiation, the cells were incubated for 24 h at 37 °C and cell viability was measured using the MTT assay.

14. *Comparisons of doxorubicin release*

To compare the effectiveness of endocytosis-mediated drug transport with that of cell membrane particle adsorption A549 cells were exposed to AuHNS, AuHNS-EGFR, AuHNS-DOX, or AuHNS-EGFR-DOX for 2 h at room temperature. A549 cells were also treated with free doxorubicin (0.5 μg/mL) for 2 h to compare the drug releasing effects. To achieve endocytosis mediated drug delivery, cells were seeded into 96-well plates (1×10^4 cells/well) after washing with PBS at least 6 times by centrifugation, and incubated for 4 h in a humidified 5% CO_2 incubator at 37 °C. NIR laser irradiation was applied to each well with 125 mW/cm^2 (diameter 2 mm, 10 s). Plates were incubated for 12 h and cell viability was measured using the MTT assay. To measure the efficiency of NPs accumulated on the cell surface, targeted cells for 2 h were seeded into 96-well plates (1×10^4 cells/well) after washing. Then, NIR laser irradiation was applied to each well. After 16 h incubation in a humidified 5 % CO_2 incubator at 37 °C, cell viability was measured by MTT assay. Two groups of AuHNS-EGFR-DOX (endocytosis inducing and

accumulation NPs on the cell surface) were compared again at different laser condition (125 mW/cm^2, diameter 7 mm, 25 s).

15. TEM images of AuHNS-EGFR-DOX treated cells

After 2 h targeting of PEGylated AuHNS and AuHNS-EGFR-DOX to lung cancer cells (3.0×10^{10}/mL, 100 μL) at room temperature, (i) half of A549 cells was washed with PBS over 6 times with 1,500 rpm for 1.5 min to retain only targeted AuHNS-EGFR-DOX; (ii) another half was added to a T75 flask and incubated 4 h in a humidified 5 % CO_2 incubator at 37 °C to induce receptor mediated endocytosis of NPs. PEGylated AuHNSs were prepared as a control   of (i) and (ii). After trypsinization of cells, TEM sample was prepared. In a fixing solution [35], the cells were fixed at 4 °C for overnight. The fixed cells were dehydrated in serial diluted ethanol (30, 50, 70, 80, 90 and 100 %). After dehydration, in a 1:1 mixture of propylene oxide and EPON resin, the cells were infiltrated at 70 °C overnight. For ultrathin sections, samples were cut by about 50 nm and mounted on copper grids. Sections were stained with lead citrate and uranyl acetate and observed with a JEM 1010 transmission electron microscope (JEOL, Tokyo, Japan).

16. Data analysis

All analysis data are given as means ± SEM. The results were analyzed by Student's *t*-test (Graphpad software, San Diego, CA, USA). *$P < 0.05$ was considered significant. **$P < 0.01$, *** $P < 0.001$ and # $P < 0.0001$ were highly significant compared to corresponding control.

Results and Discussion

1. Synthesis and characteristics of AuHNS

The metal nanoshell structures exhibit strong plasmon absorption band in the NIR region, indicating that they are promising candidate as therapeutic agents for PTT and drug delivery. The overall schematic diagram for the synthesis of target specific therapeutic agents is shown in Scheme 1. First, AgNSs (*ca.* 250 nm in diameter) were prepared by seedless and rapid growth of the Ag shell on silica NPs by the reported method of our group [36, 37]. AgNS acts as a precursor in the synthesis of AuHNS by a galvanic replacement reaction. During the galvanic replacement reaction, the Ag atoms of AgNS are galvanically replaced by Au^{3+} ions accompanying the generation of hollow interior, resulting in an increase of drug loading capacity. As-prepared AuHNSs were coated with HS-PEG-OCH$_3$/HS-PEG-COOH (molar ratio 10:1) for providing biocompatibility and further bio-conjugation sites. After the PEGylation, EGFR antibody was conjugated to the carboxyl group of PEGylated AuHNS by EDC/NHS coupling method. Lastly, doxorubicin was introduced into the AuHNS-EGFR carrier. Figure 1A shows structural and atomic composition changes from AgNS to AuHNS through galvanic replacement reaction. AuHNS shows the outer nanoshell structure (Figure 1A-a

and d) with more faint contrast than AgNS in the TEM-images due to the thinner shell of AuHNS. Moreover, homogeneous distribution of AgNS and AuHNS could be observed in TEM image (Figure 2). To observe the hollow interior of AuHNS more clearly, cross-sectional images were obtained by slicing AgNS and AuHNS with a focused ion beam. The AgNS did not have a hollow interior as shown in scanning electron microscopy (SEM) image (Figure 1A-b). In contrast, AuHNSs show hollow interior between the metal shell and the silica core particle (gap distance of approximately 16 nm) (Figure 1A-e). In addition, the Au element, detected by energy dispersive X-ray spectroscopy (EDX), appears at AuHNS after the galvanic replacement reaction (Figure 1A-c, f). Next, the plasmonic spectra of the AgNS and AuHNS were measured by UV-Vis-NIR spectrometery as shown in Figure 1B. The plasmonic band of the AuHNS was shifted toward a wavelength longer than that of the AgNS, which was attributed to the thinner shell thickness of the AuHNS in comparison with that of the AgNS due to galvanic replacement. AuHNS showed stronger absorbance in the NIR region than that of AgNS, which can be related to a higher potential for heat generation upon irradiation with NIR light [38, 39]. To confirm the photothermal effect, temperature changes of the AuHNS dispersion in PBS was measured upon irradiation using a femtosecond-pulse laser with a wavelength of 800 nm. As shown in Figure 1C, the temperature of the AuHNS dispersion (1 mg/mL) gradually increased from 24°C to 45°C ($\Delta T = 21$°C) upon NIR irradiation

(800 mW/cm^2, 10 min), whereas temperature of buffer solution was increased only 4℃ after NIR irradiation. This temperature elevation could induce cell death and make cancer cells sensitive to the effects of radiation and certain anti-cancer drugs [7]. Prior to the application of AuHNSs to cancer cells, the cytotoxicities of various concentrations of AuHNSs were measured to determine the optimal concentration of AuHNSs for PTT by the MTT assay. PEGylated AuHNSs show no toxicity in A549 cells at concentrations lower than 3×10^{10}/mL (Figure 1D).
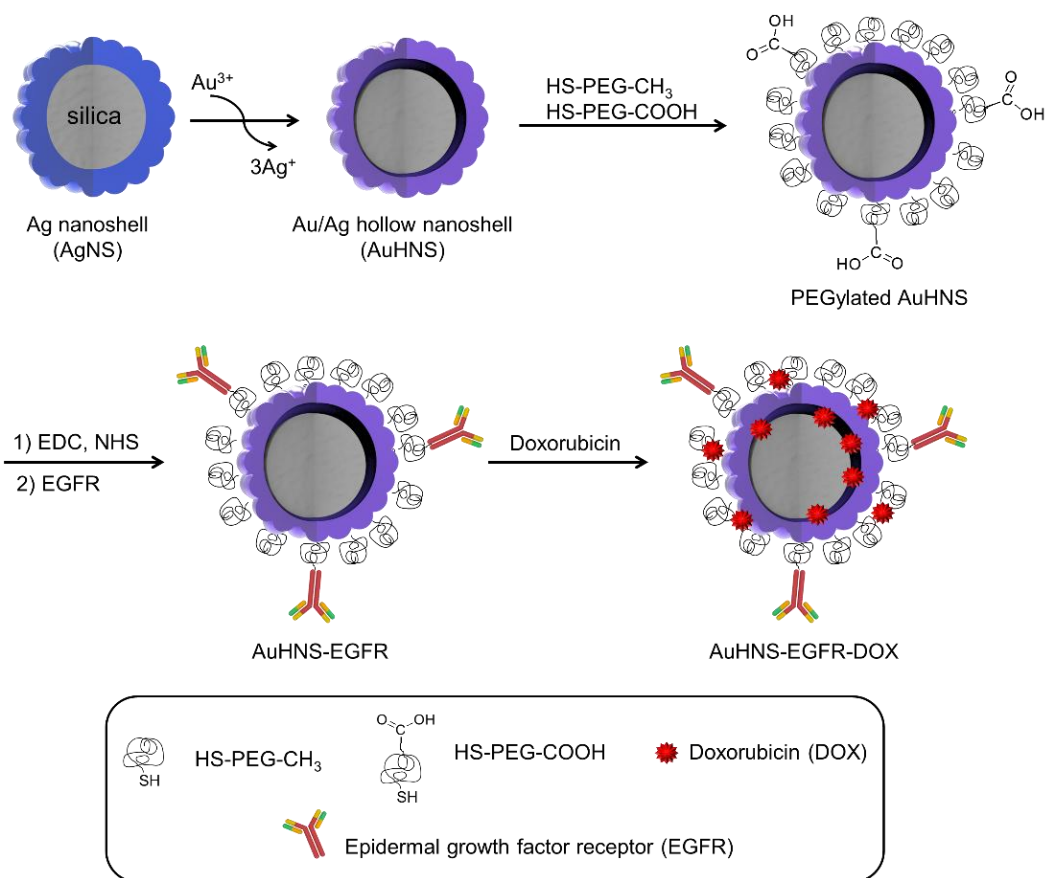
Scheme 1. Schematic illustration for the preparation of EGFR-conjugated and doxorubicin-loaded Au/Ag hollow nanoshell (AuHNS-EGFR-DOX). After the synthesis of AuHNS from the Ag nanoshell (AgNS) by galvanic replacement reaction, AuHNS was modified with poly(ethylene glycol) derivatives to allow conjugation of the EGFR antibody and increase biocompatibility. Next, EGFR antibody was conjugated through activation of the carboxyl groups at the surface of PEGylated AuHNS, followed by doxorubicin loading.

2 4
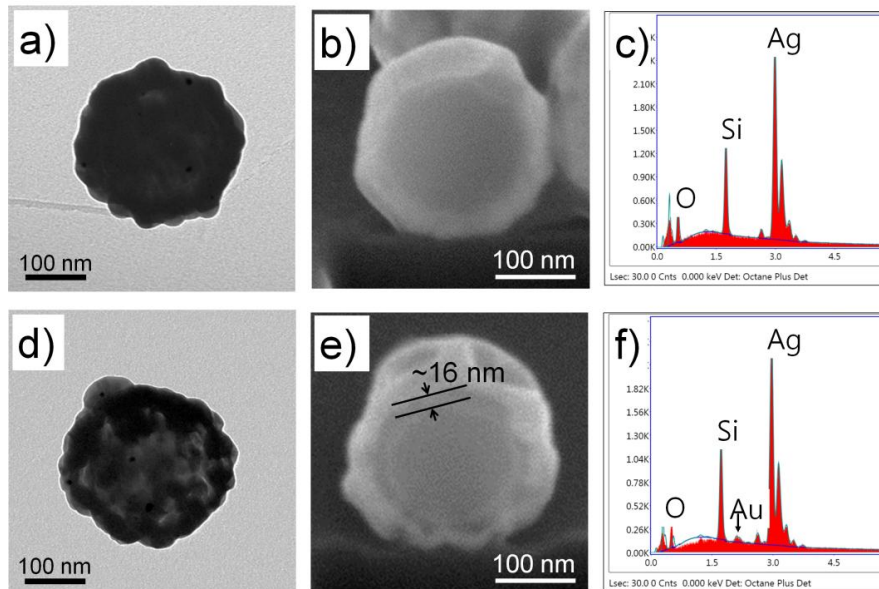
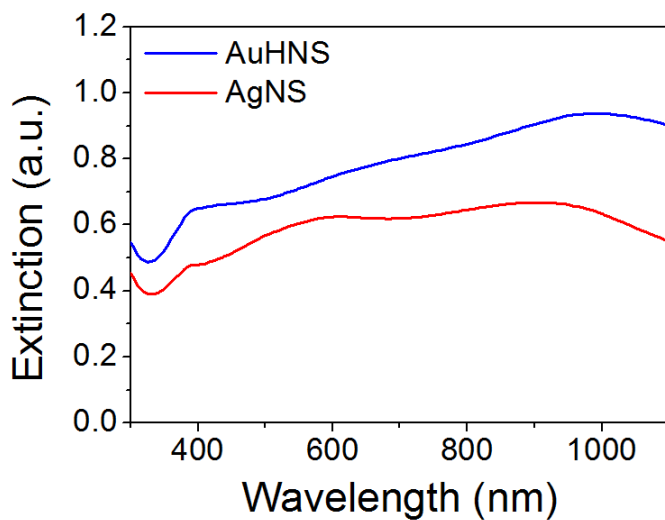**Figure 1**. **Characteristics of AgNS and AuHNS. A.** TEM images of (a) AgNS and (d) AuHNS, sectional SEM image of (b) AgNS and (e) AuHNS, and EDX spectra of (c) AgNS and (f) AuHNS. **B.** UV-Vis-NIR spectra of AgNS (red line) and AuHNS (blue line).
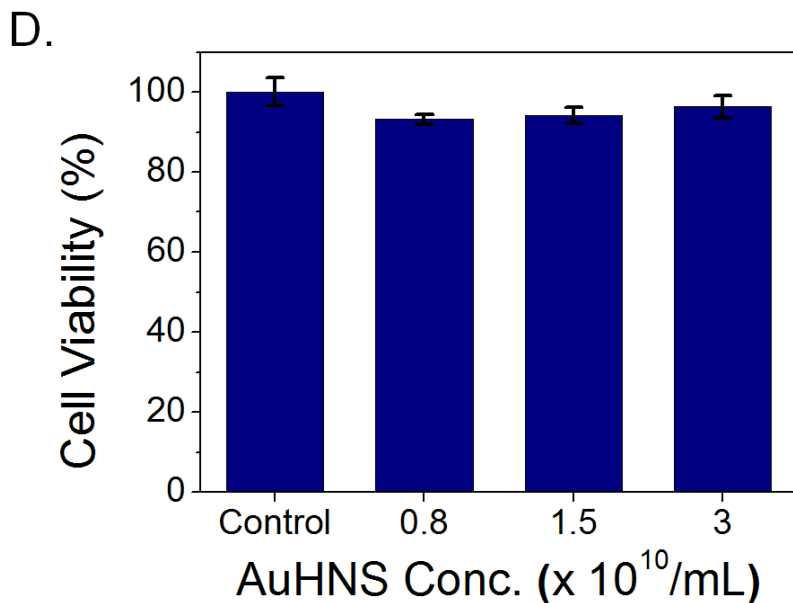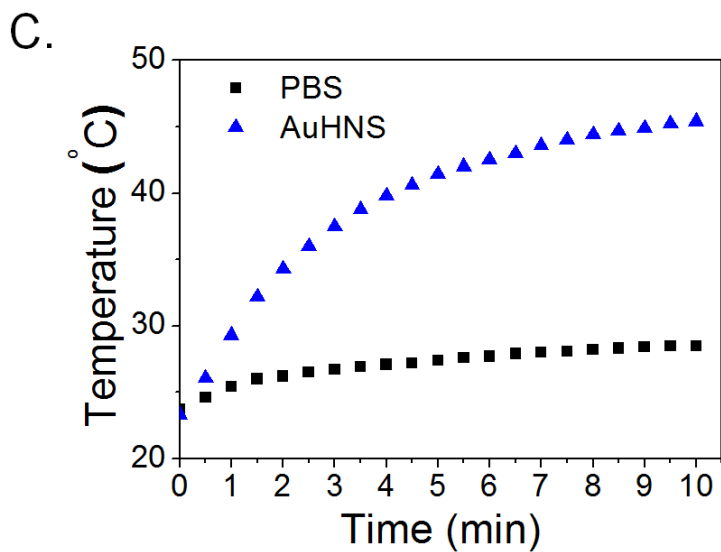
Figure 1. **Characteristics of AgNS and AuHNS. C.** Temperature elevation of aqueous AuHNS suspension (1 mg/mL) under NIR laser irradiation (800 nm, 800 mW/cm^2) for 10 min. **D.** Cell viability of AuHNS with various concentrations (0.8 × 10^{10}–3.0 × 10^{10}/mL, 100 µL) after 8 h incubation.
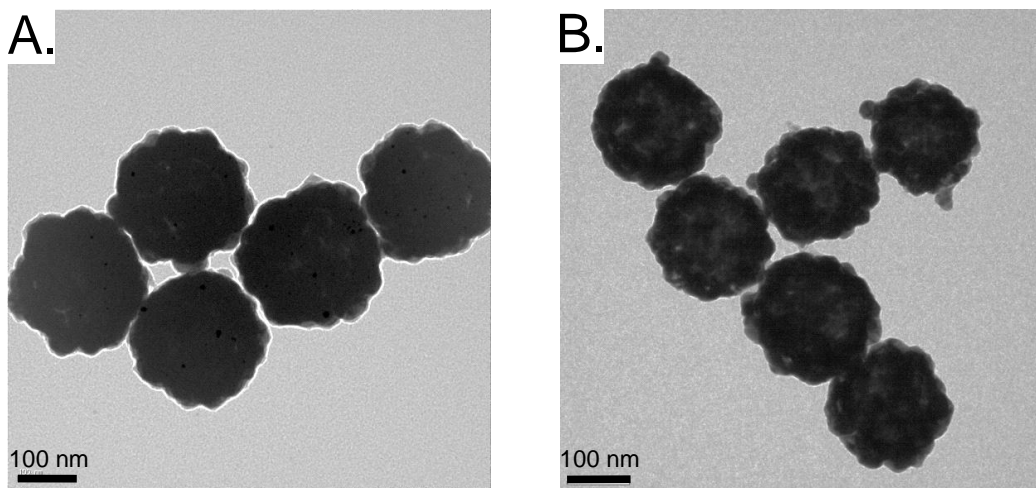
Figure 2. Homogeneous synthesis of AgNSs and AuHNS. TEM images of **A.** AgNSs and **B.** AuHNSs showing homogeneous distribution of NPs.

2. Photothermal property of PEGylated AuHNS

To verify the photothermal activity of PEGylated AuHNS, PEGylated GNR was used as a control (Figure 3A). GNR has longitudinal plasmon resonances that are highly polarization-dependent at around 780 nm (Figure 3B), and it induces a PTT *in vitro* and *in vivo* [14, 40]. However, in previous studies, GNR has been known to exhibit toxicity due to the presence of the cationic surfactant, cetyltrimethylammonium bromide (CTAB), which is a widely used surfactant for the synthesis of GNR [41, 42]. Thus, there is a need to replace the surfactant with biocompatible material such as PEG [15]. The cell viability assay was performed for PEGylated GNR and PEGylated AuHNS under the same concentrations. PEGylated GNR showed cell viability over 80 % (Figure 3C), and the cell viability of GNR-treated cells was lower than that of PEGylated AuHNS treated cells (over 90 %).

Prior to PTT of cancer cells with AuHNS and GNR, the laser power was optimized. A549 cells without NPs treatments were exposed to a femtosecond-pulse laser for 10 s, and the powers of the laser were varied (31.3, 62.5, 125, 187.5, and 250 mW/cm^2). After laser irradiation, the cells were stained with the live/dead viability/cytotoxicity kit (eth-1, CA) to visualize live and dead cells. As shown in Figure 4A, 187.5 mW/cm^2 and 250 mW/cm^2 were too strong for PTT because they caused A549 cell's death. In contrast,

laser powers of below 125 mW/cm^2 caused no cell death (Figure 4A-d, j, and p). Uptake of PEGylated AuHNS in A549 cells effectively induced cell deaths at 125 mW/cm^2 (Figure 4B-b, white arrows) and the counts of dead cells were significantly increased (Figure 4B-c). Therefore, the power of 125 mW/cm^2 was selected for NIR irradiation in PTT. The cell viability test was performed under NIR laser irradiation, and the photothermal performance of PEGylated AuHNS was compared with that of PEGylated GNR (Figure 5). To investigate the effect on cell death, A549 cells were treated with the PEGylated AuHNS or GNR, and A549 cells were then incubated for 8 h at 37 ℃. After incubation, A549 cells were exposed to a femtosecond-pulse laser with 125 mW/cm^2 power for 10 s and cell deaths were observed from trypan blue stained images (Figure 5A). The counts of dead cells after treating with PEGylated AuHNS were significantly higher than that of control cells. Cell death assays for PEGylated AuHNS and GNR exhibited similar counts (Figure 5B). These results show that PEGylated AuHNS is an effective nanomaterial for NIR PTT and can be used in various bio-applications without toxicity.

A.

50 nm

B.

C.
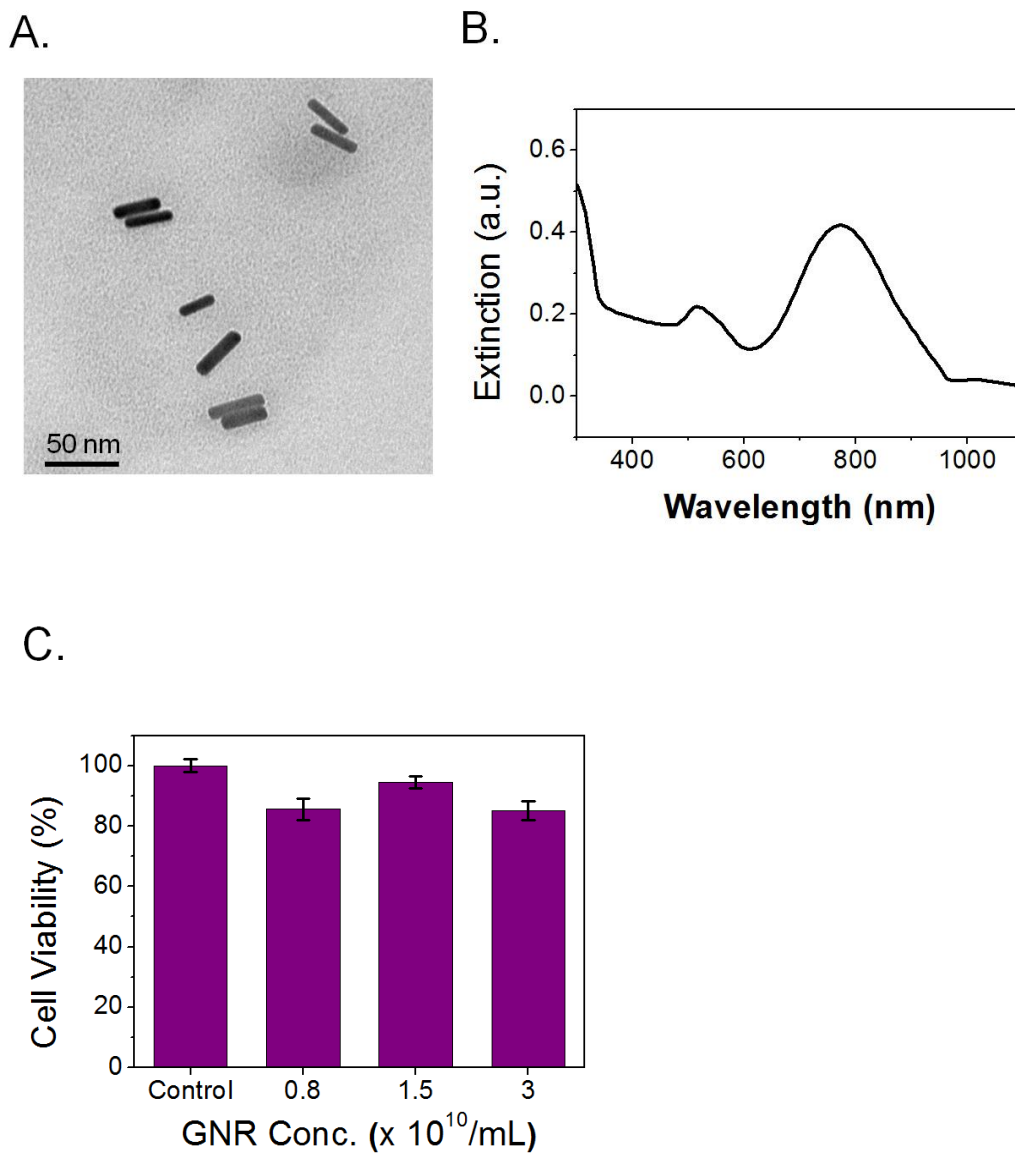
Figure 3. Characteristics of GNR. A. TEM image of gold nanorods (GNRs). **B.** UV-Vis spectrum of GNR (1 mg/mL). **C.** Cell viability with AuHNS at various concentrations.

A.

(mW/cm^2, 10s)

	Con	31.3	62.5	125	187.5	250

Live Cell

a) b) c) d) e) f)

50 μm | 50 μm | 50 μm | 50 μm | 50 μm | 50 μm

Dead Cell

g) h) i) j) k) l)

50 μm | 50 μm | 50 μm | 50 μm | 50 μm | 50 μm

Merged Image

m) n) o) p) q) r)

50 μm | 50 μm | 50 μm | 50 μm | 50 μm | 50 μm

3 1
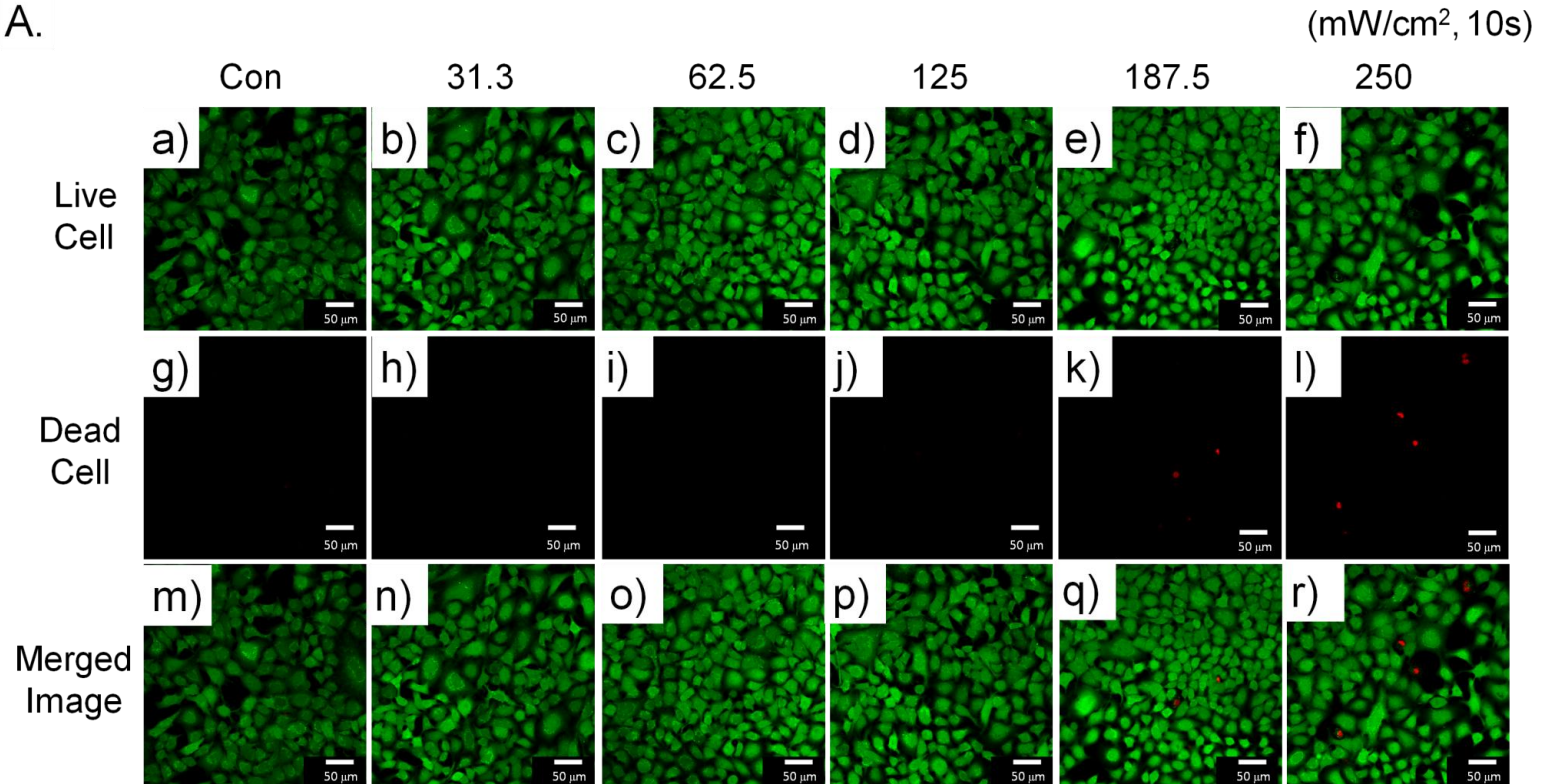
Figure 4. Decision of laser power in A549 cells. A. CLSM imaging of stained A549 cells after diverse applications of laser power to determine live and dead cells. (a-f) Images of live cells with green fluorescence. (g-l) Images of dead cells with red fluorescence. (m-r) Merged images. (a, g,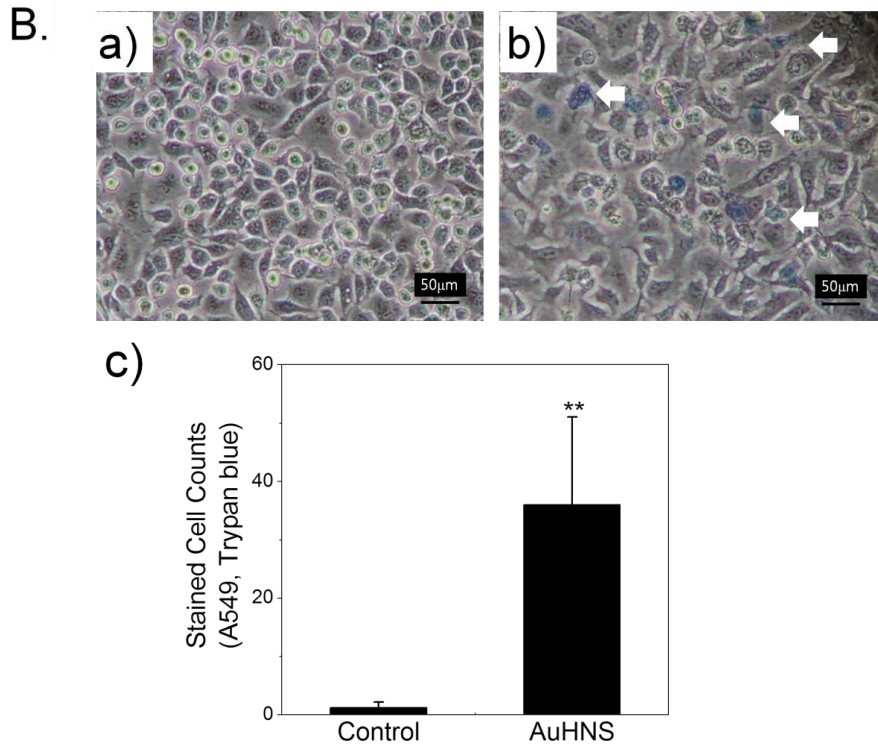 m) Control A549 cells without laser irradiation. (b, h, n)   31.3 mW/cm^2, (c, i, o) 62.5 mW/cm^2, (d, j, p) 125 mW/cm^2, (e, k, q) 187.5 mW/cm^2, and (f, l, r) 250 mW/cm^2 were administered for 10 s to an area of 2 mm in diameter. **B.** (a) Optical image of trypan blue staining after NIR irradiation (125 mW/cm^2) on A549 cells. (b) Optical image of A549 cells after treating with PEGylated AuHNS for 8 h. (c) Stained cell counts. Each bar represents the mean ± SEM (n = 4). **$p < 0.01$ compared to control cells.
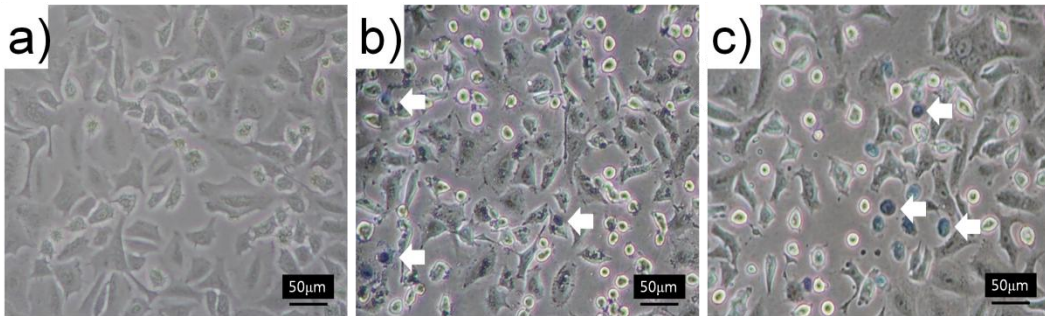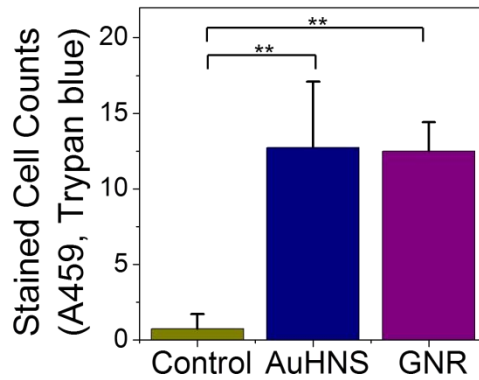
Figure 5. Comparisons of cell killing effect of PEGylated AuHNS and PEGylated GNR. A. Optical microscope images. (a) A549 control cells; (b) A549 cells with PEGylated AuHNS; and (c) A549 cells with PEGylated GNR. (a-c) Cells were treated with NIR irradiation (125 mW/cm^2, 2 mm diameter, 10 s). White arrows indicate trypan blue stained cells. **B.** Trypan blue-stained cell counts after laser exposure. Each bar represents the mean ± SEM (n = 4). **$p < 0.01$ compared to control cells.

3. Synthesis of AuHNS-EGFR-DOX

Next, we synthesized the AuHNS-EGFR-DOX for targeting specific cells, NIR triggered drug release and PTT. EGFR antibody is an ideal for targeting cancer cells because EGFR is upregulated in various cancer cells, including lung cancers, and the EGFR overexpression is related to disease progression and survival [32, 43]. Doxorubicin was chosen as a model drug to test our drug delivery system in lung cancer cells, since doxorubicin is an effective cytotoxic anticancer drug at very low concentrations [44]. First, the PEGylated AuHNS was conjugated with the EGFR monoclonal antibody using the EDC/NHS coupling method. Then, AuHNS-EGFR-DOX was prepared by simple mixing AuHNS-EGFR with doxorubicin for 24 h at room temperature. Then, it was washed completely to remove unloaded doxorubicin. After loading of doxorubicin into AuHNS-EGFR, the color of the AuHNS solution changed from brown to reddish brown. AuHNS-EGFR-DOX has three functions: targeting specific cancer cells via the EGFR antibody, PTT by NIR irradiation, and anticancer drug delivery using the hollow interior (Scheme 2A). Lung cancer cells that have many EGFR receptors on their surfaces were targeted by AuHNS-EGFR-DOX. After targeting, the cancer cells were exposed to an NIR femtosecond-pulse laser. The targeted cancer cells were thus affected by photothermal effects and released drug at the same time (Scheme 2B).
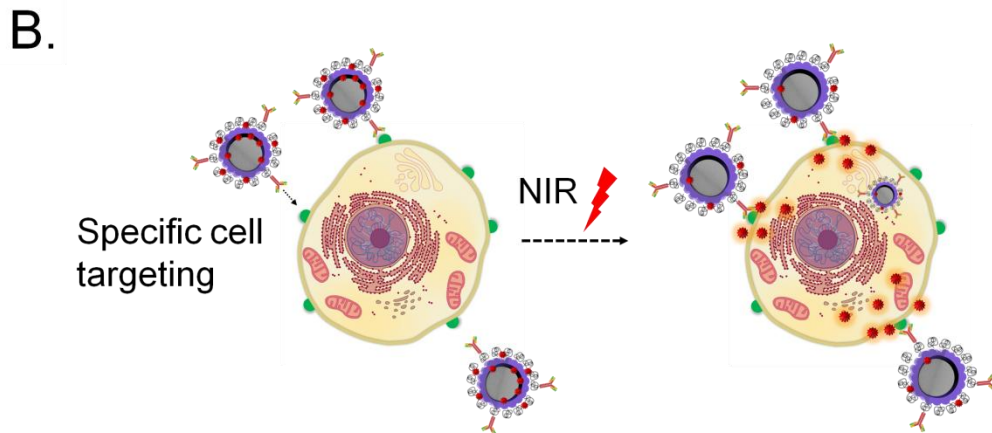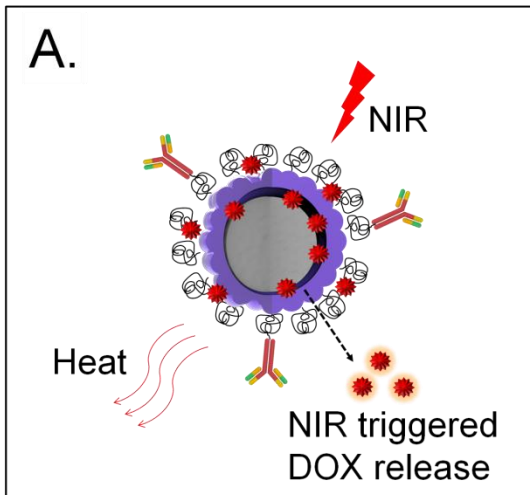
Scheme 2. Multifunctionality of AuHNS-EGFR-DOX. The doxorubicin-loaded AuHNS complexes effectively lead to specific cancer cell death through synergetic effect of **A.** NIR light triggered doxorubicin release and heat generation, and **B.** Specific cancer cell targeting.

4. Targeting efficiencies of AuHNS-EGFR and AuHNS-EGFR-DOX

The conjugation of the EGFR antibody to AuHNS was confirmed by the dot blotting method with secondary antibody-HRP detection on the nitrocellulose membrane. The AuHNS did not show any chemiluminescent signals after HRP detection, whereas EGFR-conjugated AuHNS was detected with HRP and showed SNU logo-shaped chemiluminescent signals (Figure 6A). To determine the optimal cell-line for verifying the targeting ability of AuHNS-EGFR-DOX, we evaluated the expression of EGFR in A549 and H522 cells. As shown in Figure 6B, A549 cells overexpressed EGFR, however, H522 was null for EGFR. This result is consistent with previous reports that investigated the quantity of EGFR in lung cancer cells [43, 45, 46]. Dark-field microscope images of A549 and H522 cells after targeting with AuHNS-EGFR, and AuHNS-EGFR-DOX are shown in Figure 6C. The targeted A549 cells show shiny orange dots at the cell membranes where EGFR is expressed, due to light scattered from AuHNS (Figure 6C-c). In the H522 cells, there were very few shiny dots of AuHNS (Figure 6C-d). These results indicate that AuHNS-EGFR targets specifically A549 cells without nonspecific binding. The same result was obtained in the case of AuHNS-EGFR-DOX, suggesting that the targeting ability of the AuHNS-EGFR-DOX was maintained after doxorubicin loading

(Figure 6C-e and f). From these results, we confirmed that AuHNS-EGFR-DOX could

specifically target A549 cells in comparison with H522 cells. This targeting ability could

minimize side effects caused by nonspecific binding of NPs.
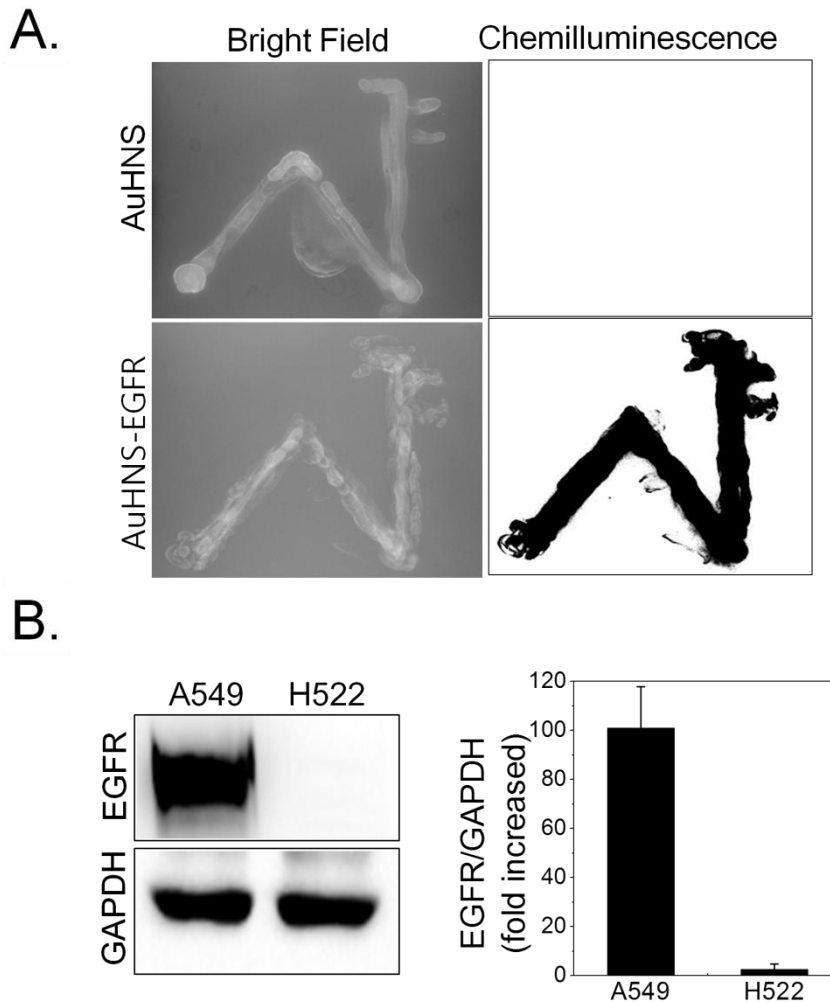
Figure 6. Targeting efficiency of EGFR antibody-conjugated AuHNS. A. HRP detection of AuHNS and AuHNS-EGFR on nitrocellulose membrane. **B.** Comparisons of EGFR levels in A549 and H522 cells. Bands are representative of three individuals from each group. Densitometric analysis of western blots (lower location). Each bar represents the mean ± SEM (n = 3).

Figure 6. Targeting efficiency of EGFR antibody-conjugated AuHNS. C. Light-scattering images of A549 (a, c, e) and H522 cells (b, d, f). The images show A549 and H522 cells (a, b), cells exposed to AuHNS-EGFR (c, d), and cells exposed to AuHNS-EGFR-DOX (e, f). Yellow shiny spots indicate the NPs.

5. *Drug releasing abilities of AuHNS-EGFR-DOX*

The doxorubicin loading and release properties of doxorubicin-loaded AuHNS under various conditions were evaluated. UV-Vis spectra revealed that a 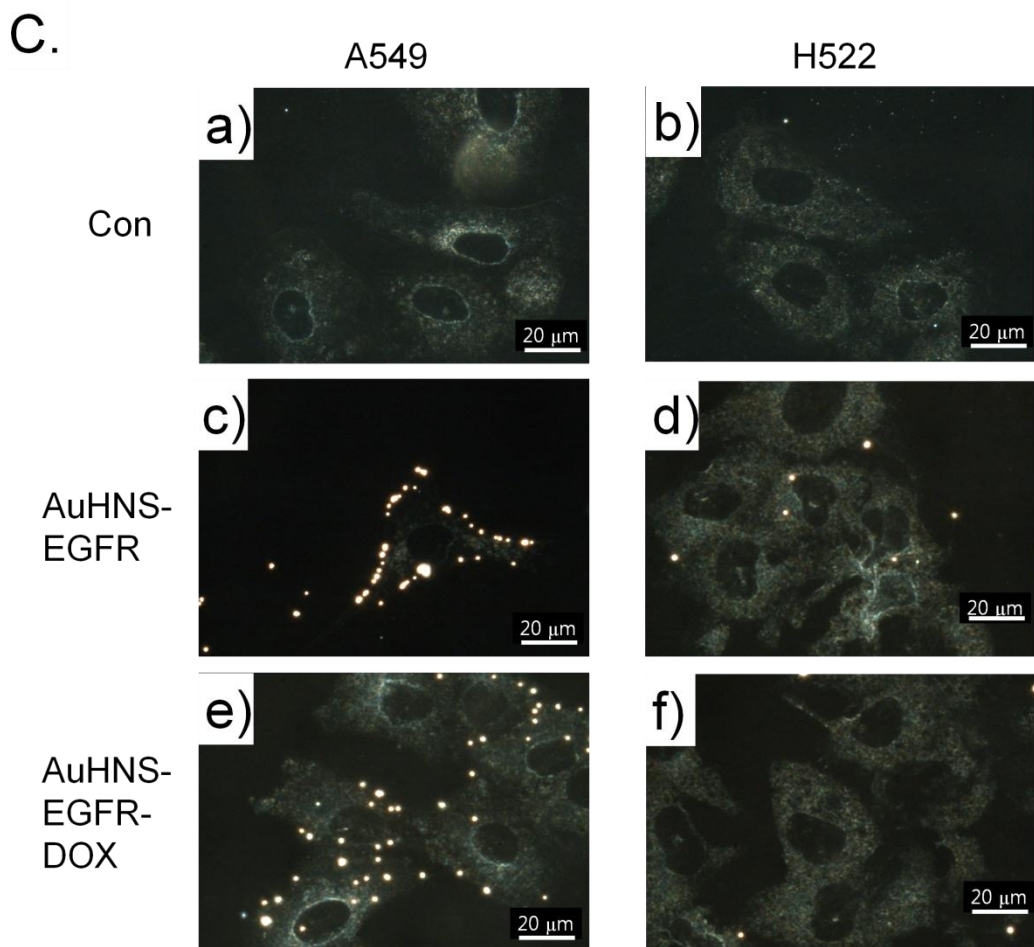peak around 480 nm corresponding to doxorubicin newly appeared after doxorubicin loading into AuHNS (Figure 7). The amount of doxorubicin loaded into the AuHNS was estimated by measuring the absorbance at 480 nm. The doxorubicin loading capacity of AuHNS was approximately 3×10^6 DOX molecules per single AuHNS particle (Figure 8), which is greater than the capacity of conventional AuNPs [47]. The hollow structure of AuHNS could promote doxorubicin loading inside its hollow interior spaces. In addition, the surface of AuHNS could adsorb hydrophobic doxorubicin by hydrophobic interactions. Next, release of the loaded doxorubicin was observed at different pH conditions (pH 5.0 and pH 7.4) by measuring UV-Vis absorption of doxorubicin from a supernatant after precipitating AuHNS. As shown in Figure 7B, AuHNS-DOX was relatively stable at pH 7.4 so that doxorubicin was scarcely released during 24 h. In contrast, at pH 5.0, around 10 % of the doxorubicin was released in 2 h, and up to 12 % over 24 h, which is due to the increased water solubility of doxorubicin under acidic condition. DOX release profiles at pH 5.0 and 7.4 were significantly different due to the electronic repulsion between DOX and the carriers [48]. These results suggest that doxorubicin-loaded

AuHNS nanocarriers are stable at neutral pH environment [49], and could release doxorubicin under a cancer cell environment (at pH 5.0). The doxorubicin release from AuHNS-DOX under NIR irradiation of 125 mW/cm^2 power was evaluated (Figure 7C). Doxorubicin release was boosted to 12 % after 4 h NIR irradiation, but the non-irradiated group showed small amount of doxorubicin release in a non-triggered manner. Therefore, doxorubicin release from AuHNS can be controlled by NIR laser-triggering and pH change. Next, to verify the therapeutic effect of doxorubicin loaded AuHNS against cancer cells, A549 cells were incubated with three kinds of AuHNS based particles (AuHNS, AuHNS-EGFR, and AuHNS-EGFR-DOX) at 37℃ for 48 h (Figure 7D). AuHNS-EGFR treated A549 cells showed slightly decreased cell viability in comparison with AuHNS treated cells, but the cell viability was over 80 %. AuHNS-EGFR-DOX induced a significant decrease in cell viability to less than 40 % after A549 cells were treated for 48 h. These results suggest that AuHNS-EGFR-DOX can kill the specific cancer cells by effective drug delivery with specific targeting.
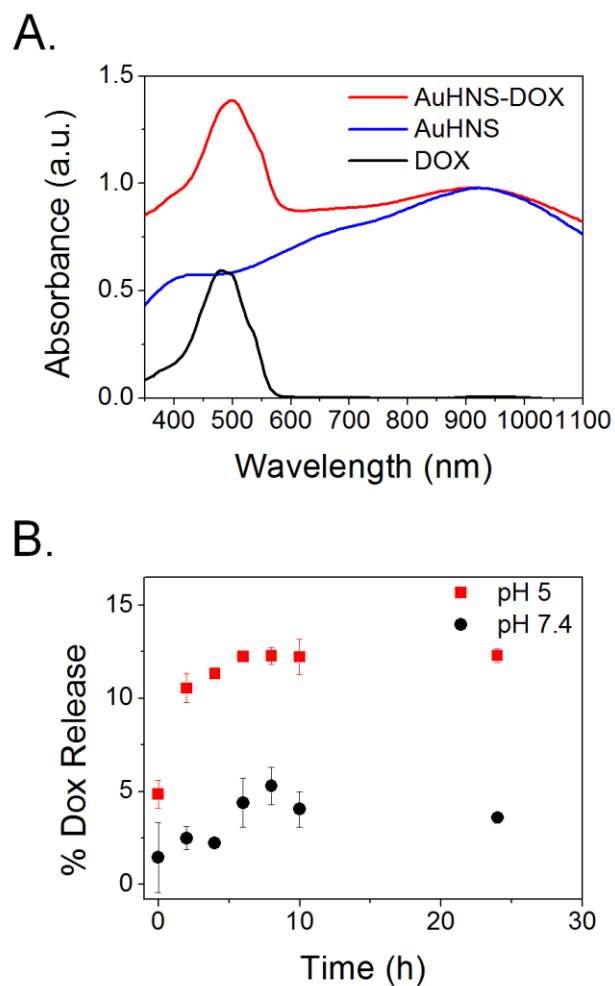
Figure 7. Drug releasing abilities of AuHNS-EGFR-DOX. A. UV-Vis spectra of AuHNS-EGFR-DOX (0.02 mg/mL), AuHNS (0.02 mg/mL), and free DOX (60 μM) showing loading of DOX to AuHNS. **B.** Doxorubicin release profile of the AuHNS-DOX (0.1 mg/mL) at different pH. Doxorubicin was not released at pH 7.4, but was released at pH 5.
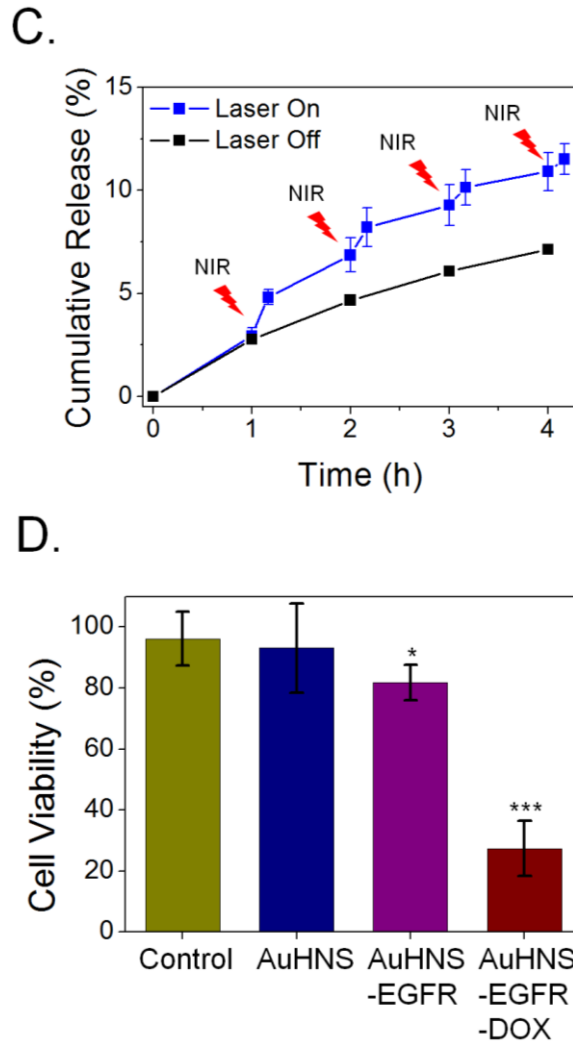
Figure 7. Drug releasing abilities of AuHNS-EGFR-DOX. C. Induced release of doxorubicin from AuHNS-DOX (1 mg/mL) by NIR irradiation (800 nm) was observed at pH 7.4. Doxorubicin was released in a NIR light-controlled manner. **D.** Quantitative cell viability results of A549 cells treated with different AuHNS complexes for 48 h. AuHNS-EGFR-DOX decreased cell viability to less than 40 %, whereas AuHNS and AuHNS-EGFR showed no cytotoxicity. Each bar represents the mean ± SEM (n = 4). *: $p<0.05$, and ***: $p < 0.001$.
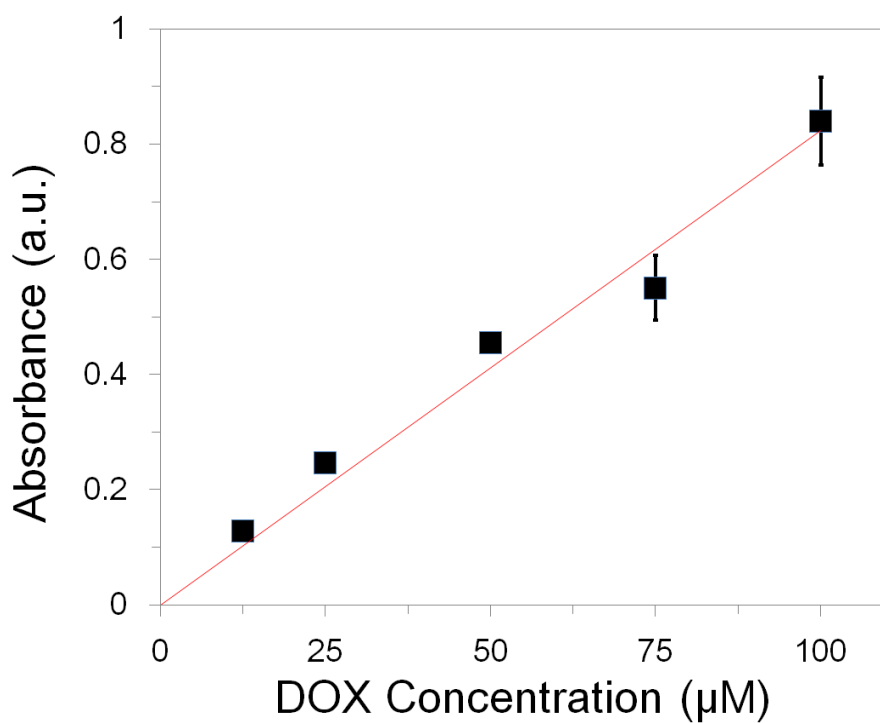
Abs. (a.u.) = 0.0082 x [DOX]
R^2=0.9707

[DOX] (µM) = 121.9 x Absorbance

Figure 8. Calibration curve of doxorubicin aqueous solution as a function of concentration. Absorbance was measured at 480 nm.

6. Mechanism of drug delivery system I: receptor-mediated endocytosis

Therapeutic efficacies of the PEGylated AuHNS to lung cancer were compared by two targeting methods through maximizing the ability of targeting to cancer cells, drug release and thermotherapy by NIR irradiation (Figure 9). First, we focused on receptor-mediated endocytosis after targeting AuHNS-EGFR-DOX to A549 cells. Various kinds of NPs have been reported to be able to enter cells by endocytosis pathways, which may be mediated by clathrin, caveolae, macropinocytosis, or phagocytosis [24, 50-52]. Based on this endocytosis property, doxorubicin-loaded NPs have been commonly applied for drug delivery [19, 24, 28, 35, 53]. Figure 9A shows the scheme for doxorubicin delivery by receptor-mediated endocytosis in A549 cells. After A549 cells were treated with AuHNS-EGFR-DOX for 2 h at room temperature, AuHNS-EGFR-DOX bound A549 cells were incubated for 4 h at 37 °C to induce receptor-mediated endocytosis. To observe the NIR irradiation effects, one group of A549 cells was exposed to 800 nm irradiation (2 mm diameter) for 10 s with 125 mW/cm^2 and incubated for 12 h. Another group was treated by the same method except NIR laser exposure. The results of the MTT assay are shown in Figure 9B. The cell viability of the NIR irradiation group (blue bars) was generally lower than the group without NIR irradiation (gray bars). When AuHNS-DOX and

AuHNS-EGFR-DOX are compared, AuHNS-EGFR-DOX is more effective to kill cancer cells. From the results, we conclude that receptor-mediated endocytosis to kill cancer cells is more effective than non-specific cellular uptake [53]. NIR laser exposure with AuHNS-EGFR-DOX significantly reduced cell viability to less than 50%. In the case of free doxorubicin, similar reduction of cancer cells (approximately 55 %) occurred at the concentration of 0.5 μg/mL.

A. Receptor-mediated endocytosis for drug release

Specific cell targeting

B.
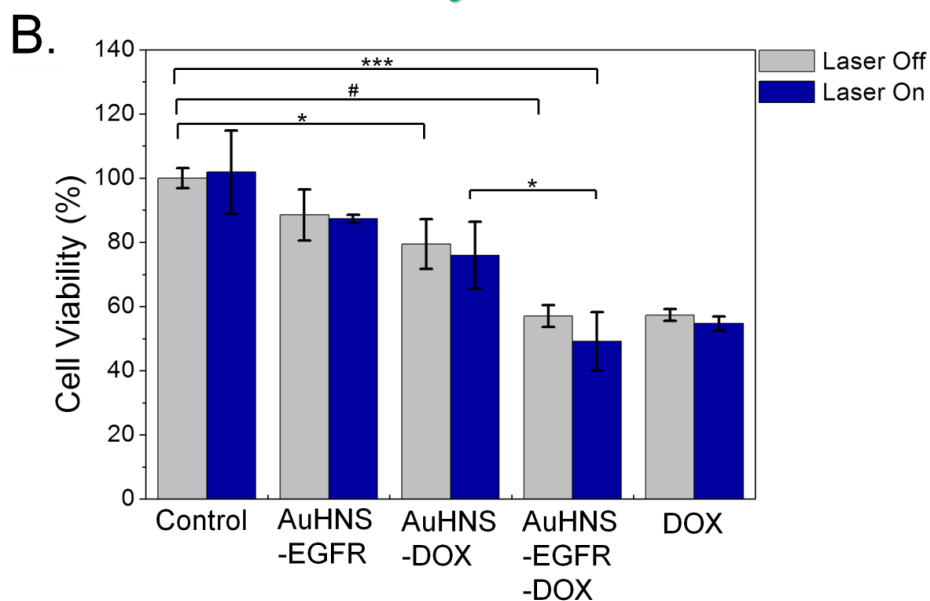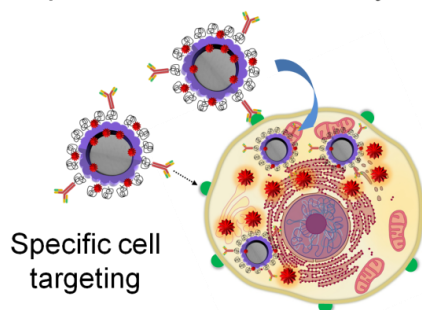
Figure 9. Cell survival from different assays using AuHNS complexes: Receptor-mediated endocytosis. A. The drug delivery scheme for cellular uptake by receptor-mediated endocytosis. A549 cells were exposed to AuHNS-EGFR-DOX, and incubated in 5 % CO_2 at 37 ℃ to induce uptake of AuHNS-EGFR-DOX. At that time, NIR laser was used to trigger drug release in the intracellular area. **B.** Cell viability of the assay from the scheme A. Gray bars indicate that the laser was not used, and blue bars indicate that the laser was used. Each bar represents the mean ± SEM (n = 4). *: $p < 0.05$, **: $p < 0.01$, ***: $p < 0.001$, and #: $p < 0.0001$.

7. Mechanism of drug delivery system II: targeted and accumulated AuHNS-EGFR-DOX on the cell membrane

We also varied the time at which NIR irradiation was applied. A549 cells were treated with AuHNS complexes for 2 h at room temperature, and then they were exposed to NIR irradiation at 800 nm. In these cases, a large amount of AuHNS complexes was located on the surface of the A549 cells by targeting EGFRs which are located to the cell surfaces (Figure 10A). In order to compare these results with those obtained using the first method (*3.3.6*), the total AuHNS complex treatment time was set equal; thus, A549 cells were incubated for 16 h at 37 ℃ after irradiation. In addition, these groups were divided into two, with NIR irradiation and without NIR irradiation. These results are shown in Figure 10B. Generally the cell viability of a group treated with the NIR laser (blue bars) was lower than that of the group without NIR irradiation (grey bars). With the AuHNS-EGFR, targeting to A549 cells showed more significant killing effects on the cancer cells after NIR irradiation when compared without NIR irradiation. The thermal therapeutic effects through NIR irradiation were dramatically increased with targeted and accumulated AuHNS-EGFR at the cell surfaces. In addition, the cell viabilities after AuHNS-DOX and AuHNS-EGFR-DOX treatment were lower than those of the figure 9 groups (AuHNS-DOX and AuHNS-EGFR-DOX). Significantly enhanced anticancer effects were observed

in the AuHNS-EGFR-DOX group, which showed the cell viability of approximately

35 %. AuHNS-EGFR-DOX showed a dramatic ability to kill lung cancer cells and was

more effective than AuHNS-DOX and free doxorubicin. The similar cell viabilities were

observed under different irradiation conditions (125 mW/cm^2, 25 s, diameter 7 mm), as

shown in the Figure 11. Therefore, by targeting EGFR on the surface of A549 cells,

chemo-thermo therapeutic effects of accumulated NPs with exposure of laser were

optimized for lung cancer treatment with AuHNS-EGFR-DOX complex.

Previous reports on the drug delivery carriers were focused on endocytosis to overcome

hydrophobicity [54] and multi-drug resistance cells (MDR) [24]. Recently, generating a

high drug concentration on the cell membrane was reported [7]. The cytotoxicities of

targeted AuHNS-EGFR-DOX are related to the accumulations of AuHNS-EGFR-DOX

on the cell membranes. In addition, the drug delivery system that enables the drug to

reach tumor cells is very important for effective chemotherapy [55].

The live and dead cell images after NIR irradiations on AuHNS complex targeted A549

cells (2 h) are shown in Figure 12. Although free doxorubicin treatment did not show cell

death after irradiation of NIR laser (Figure 12-f, l, and r), AuHNS-DOX-EGFR (Figure

12-e, k, and q) targeted A549 cells showed cell deaths right after exposure of NIR laser.

Taken together, these results show that the accumulation of doxorubicin on the cancer

cell membrane is an effective therapeutic strategy for diffusion of the drug within the cells.

For a better understanding of the laser-induced photothermal effects using the two different drug delivery systems, CLSM images to observe live and dead cells were compared before and after NIR irradiations (125 mW/cm^2, 10 s, 2 mm diameter) in AuHNS-EGFR-DOX treated cells (Figure 13). In two drug delivery cases, cell death started by inducing endocytosis for 4 h (total time: 6 h) (Figure 13B-a, c, e) or by targeting for 2 h without laser irradiation (Figure 13C-a, c, e). When exposed to laser irradiation after AuHNS-EGFR-DOX treatment, the cell death was immediately increased more than before (Figure 13B, C-b, d, f).

A. Targeting and drug release on cell surfaces

Specific cell targeting

B.
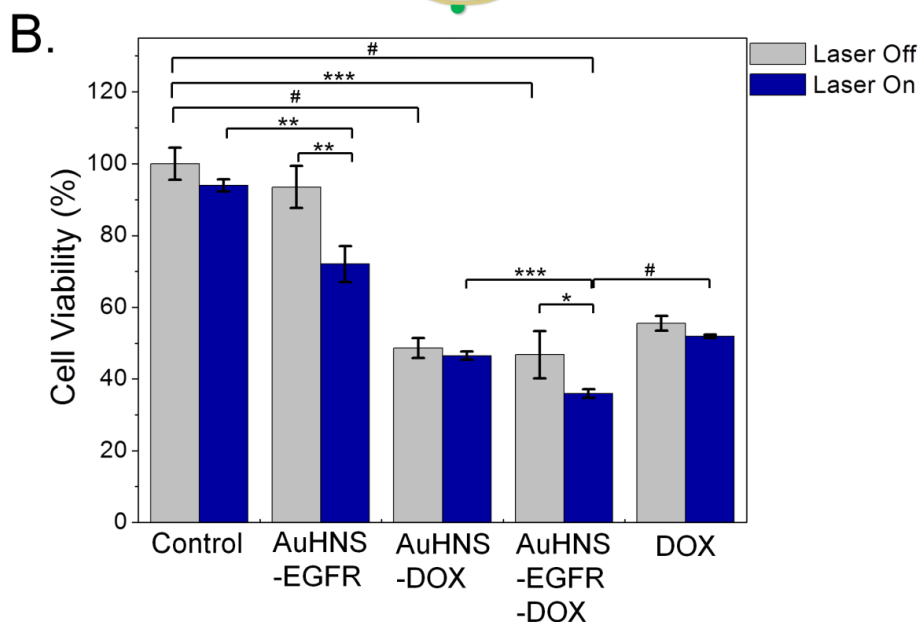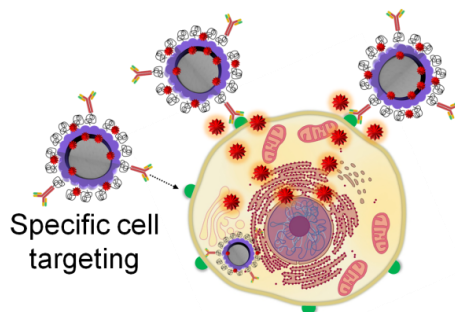
Figure 10. **Cell survival from different assays using AuHNS complexes: Accumulated AuHNSs on cancer cell membranes. A.** The drug delivery scheme for targeting cell membrane. A549 cells were treated with AuHNS-EGFR-DOX for 2 h at room temperature. An NIR laser was used to trigger drug release from the accumulated AuHNS complexes on the cell surfaces. **B.** Cell viability of the assay from the scheme A. Gray bars indicate that the laser was not used, and blue bars indicate that the laser was used. Each bar represents the mean ± SEM (n = 4). *: $p < 0.05$, **: $p < 0.01$, ***: $p < 0.001$, and #: $p < 0.0001$.
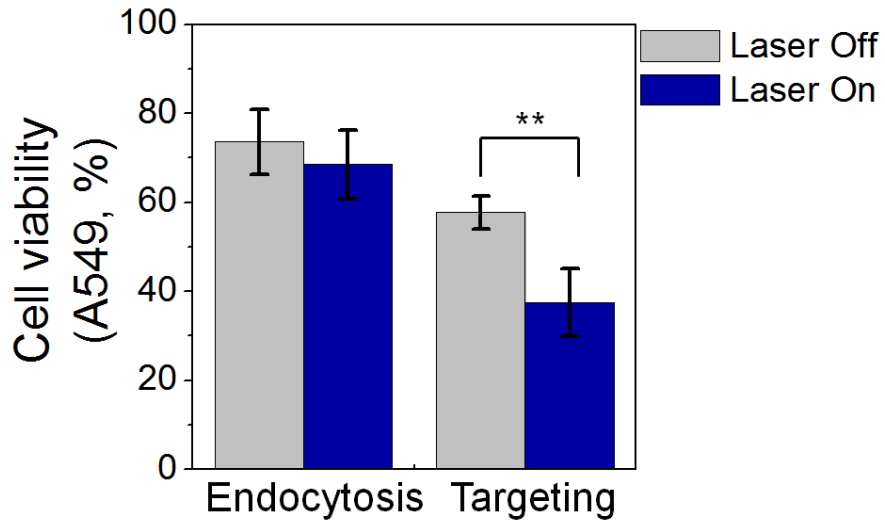
Figure 11. Viability of A549 cells treated with AuHNS-EGFR-DOX with/without laser irradiation (125 mW/cm^2, 25 s, 7 mm diameter). Left group were AuHNS-EGFR-DOX to induced receptor mediated endocytosis, whereas the right group was targeted with AuHNS-EGFR-DOX to the cell membrane by binding for 2 h. The grey bars indicate AuHNS-EGFR-DOX without NIR irradiation, and the blue bars indicate AuHNS-EGFR-DOX with NIR irradiation. Each bar represents the mean ± SEM (n = 4). **$p < 0.01$ compared with the control cells.
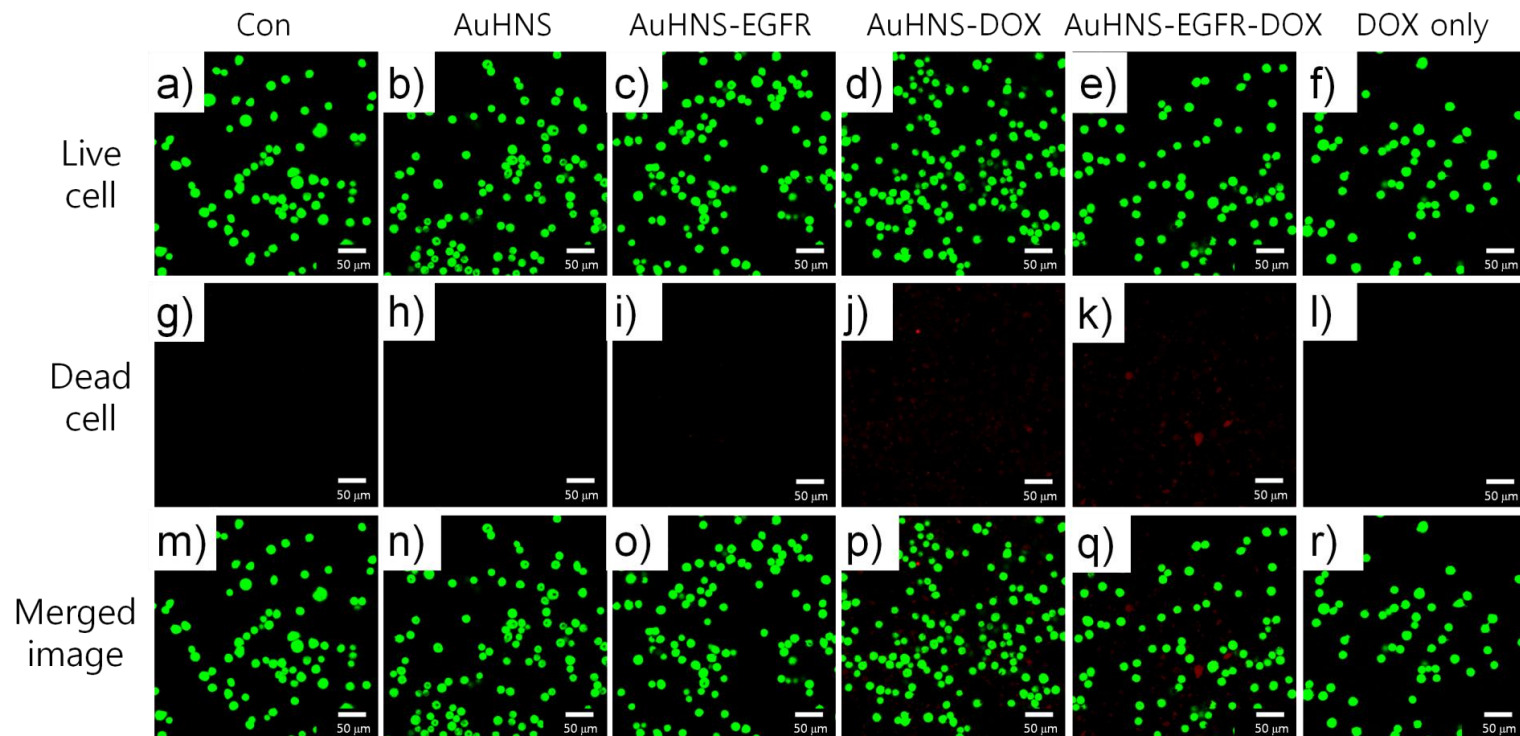
Figure 12. CLSM images of stained A549 cells after 125 mW/cm^2 irradiation for 10 s (2 mm diameter area) to the targeted AuHNS complex. (a-f) Images of live cells with green fluorescence. (g-l) Images of dead cells with red fluorescence. (m-r) Merged images. (a, g, m) Control A549 cells; (b, h, n) AuHNS; (c, i, o) AuHNS-EGFR; (d, j, p) AuHNS-DOX; (e, k, q) AuHNS-EGFR-DOX; and (f, l, r) doxorubicin only.

Figure 13. CLSM images of live and dead A549 cells following treatment with AuHNS-EGFR-DOX in the presence or absence of laser irradiation (125 mW/cm^2, 10 s, 2 mm diameter). A. Control cells without AuHNS-EGFR-DOX. The left line of each group contains cells that did not undergo laser irradiation (a, c, e), whereas the right line of each group was exposed to laser irradiation (b, d, f). Green fluorescence indicates live cells (a, b; all groups). Red fluorescence indicates dead cells (c, d; all groups). Merged images (e, f; all groups).
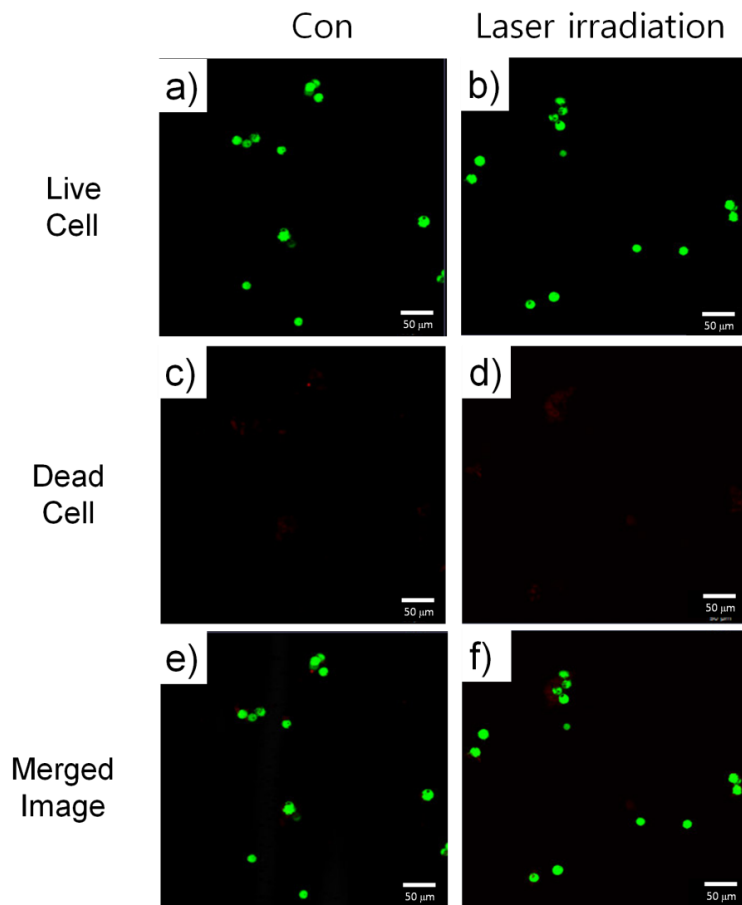
Figure 13. CLSM images of live and dead A549 cells following treatment with AuHNS-EGFR-DOX in the presence or absence of laser irradiation (125 mW/cm^2, 10 s, 2 mm diameter). B. Cells treated with AuHNS-EGFR-DOX to induce receptor-mediated endocytosis (2 h targeting; 4 h incubation in 5 % CO$_2$ at 37 °C). The left line of each group contains cells that did not undergo laser irradiation (a, c, e), whereas the right line of each group was exposed to laser irradiation (b, d, f). Green fluorescence indicates live cells (a, b; all groups). Red fluorescence indicates dead cells (c, d; all groups). Merged images (e, f; all groups).
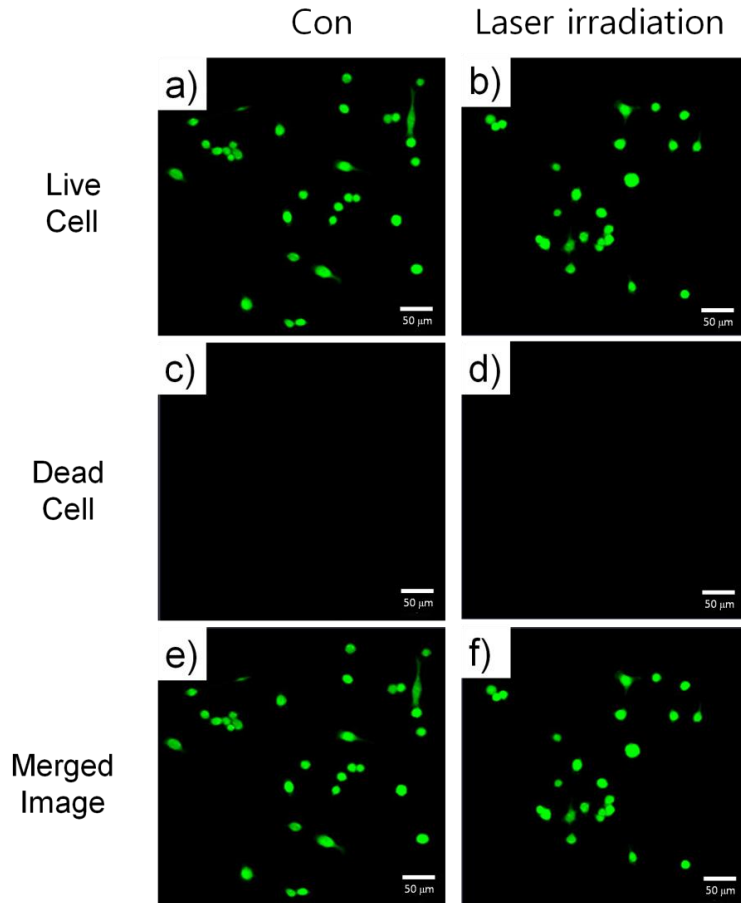
Figure 13. CLSM images of live and dead A549 cells following treatment with AuHNS-EGFR-DOX in the presence or absence of laser irradiation (125 mW/cm^2, 10 s, 2 mm diameter). C. Cells undergoing membrane targeting of AuHNS-EGFR-DOX (2 h).   The left line of each group contains cells that did not undergo laser irradiation (a, c, e), whereas the right line of each group was exposed to laser irradiation (b, d, f). Green fluorescence indicates live cells (a, b; all groups). Red fluorescence indicates dead cells (c, d; all groups). Merged images (e, f; all groups).
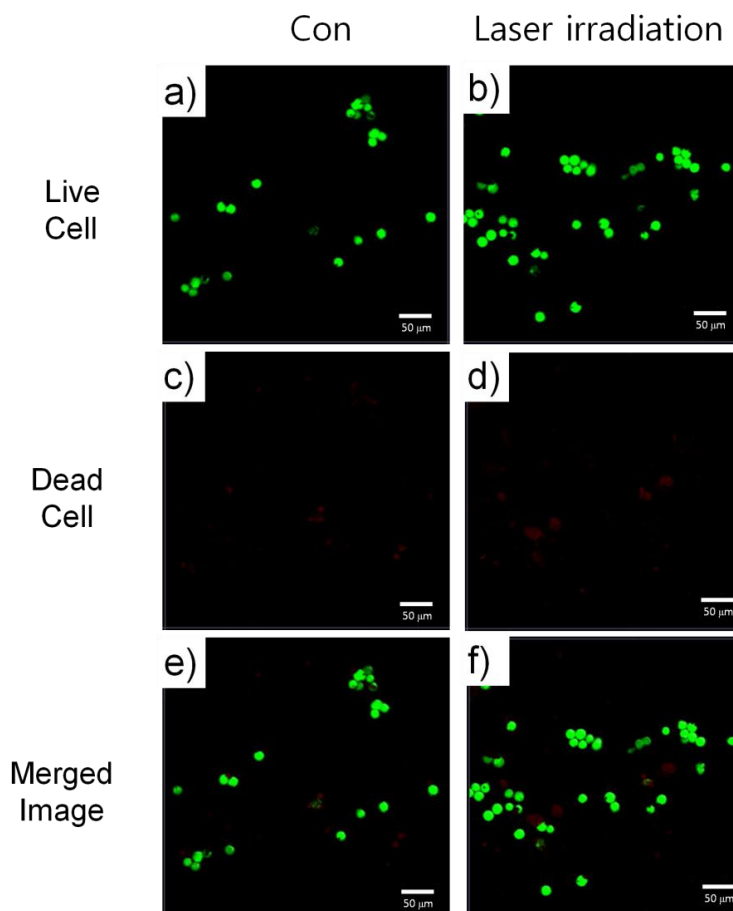
8. Verifications of cellular uptake and targeting of AuHNS-EGFR-DOX

To confirm the cellular uptake and targeting of the AuHNS complex in A549 cell, sectional TEM of AuHNS-EGFR-DOX-treated A549 cells was observed, as shown in Figure 14. Before AuHNS treatment, A549 cells showed clear cellular organelles, as shown in Figure 14A-a. To evaluate the effects of EGFR and doxorubicin on the drug delivery systems, PEGylated AuHNS and AuHNS-EGFR-DOX were administered as a control. AuHNS NPs were observed inside the cytoplasm from incubated cells for 4 h at 37 ℃ after targeting for 2 h (Figure 14A-b). Figure 14A-c is the result without 4 h incubation after targeting; there was rarely uptake of NPs into the cells. Therefore, 4 h incubation is enough to induce endocytosis into cells and 2 h targeting is appropriate to avoid non-specific binding. Figure 14B shows a large amount of AuHNS-EGFR-DOX inside of the A549 cell caused by receptor mediated endocytosis. In addition, destruction of cellular organelles such as mitochondria was observed in the A549 cell, which was induced by receptor-mediated endocytosis of AuHNS-EGFR-DOX (blue arrows in Figure 14B-c). TEM images of AuHNS-EGFR-DOX-treated A549 cell for targeting are shown in Figure 14C. There were several targeted NPs on the cell surfaces, but no AuHNS-EGFR-DOX uptake (red arrows in Figure 14C-a and b). In this group, destruction of

mitochondria with swelling and cristae breakage was observed by released DOX into the

cell (Figure 14C-c). These results show that targeted drug carriers on cell membranes

could make damages to cancer cells without internalization of the carriers.
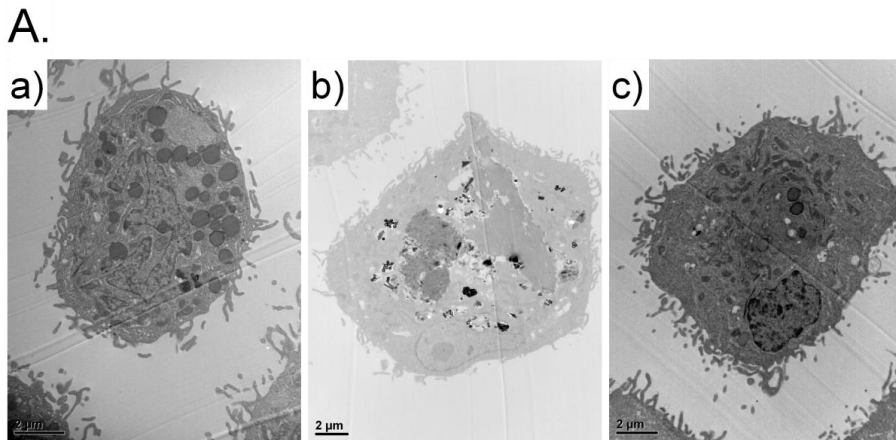
Figure 14. **TEM images of A549 cells treated with AuHNS complexes. A.** Control images of A549 cells and the PEGylated AuHNS treated group. (a) Control image of an A549 cell only. (b) An A549 cell with PEGylated AuHNSs which were targeted for 2 h and incubated for 4 h in 5 % CO_2 at 37 °C. (c) A549 cells treated with PEGylated AuHNSs for 2 h.
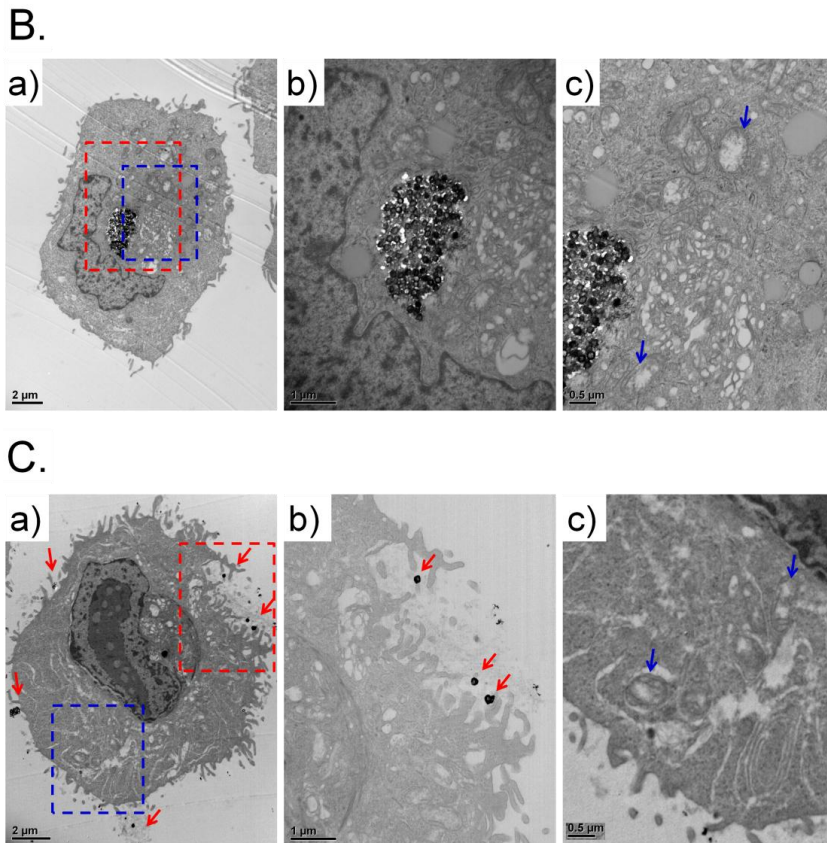
Figure 14. TEM images of A549 cells treated with AuHNS complexes. B. Cells treated AuHNS-EGFR-DOX with same protocol of A(b) to induce receptor mediated endocytosis. (b) The area of the red square was enlarged to confirm the endocytosis of AuHNS-EGFR-DOX. (c) An enlarged image of the blue square to observe changes in cell organelles (Blue arrow, mitochondria morphology with swelling and cristae breakage). **C.** Cells treated with AuHNS-EGFR-DOX for 2 h. (b) The red square area was enlarged to confirm the targeted AuHNS-EGFR-DOX at the cell surfaces. (c) An enlarged image of the blue square to observe the changes in cell organelles (Red arrows, AuHNS-EGFR-DOX at the A549 cell membrane, Blue arrows; mitochondria morphology with swelling and cristae breakage).

6 0

Conclusion

In this study, EGFR antibody-conjugated and doxorubicin-loaded AuHNS (AuHNS-EGFR-DOX) was prepared for cancer cell-targeting and drug delivery. These monodisperse nanocarriers showed multifunctional: targeting specific cancer cells and inducing anticancer effects upon NIR irradiation. Especially, the hollow interior and strong photothermal activity of these nanocarriers permitted a significant increase in doxorubicin loading as well as controlled and selective release when stimulated with NIR light.

In addition, two different drug delivery systems, induced endocytosis and drug accumulation on the cell surface, were examined to optimize the cytotoxic effects of AuHNS-EGFR-DOX. Targeted accumulation of AuHNS-EGFR-DOX on the cell membrane was more effective than receptor-mediated endocytosis and free doxorubicin. Our data revealed that NIR-induced drug release of targeted nanocarrier AuHNS-EGFR-DOX on cell surfaces was optimal with synergetic effects for treating lung cancer. Thus, AuHNS-derived nanocarriers are a promising drug-delivery system for the treatment of lung cancer and other diseases that require specific drug targeting.

References

[1] Piao Y, Burns A, Kim J, Wiesner U, Hyeon T. Designed Fabrication of Silica-Based Nanostructured Particle Systems for Nanomedicine Applications. *Adv Funct Mater.* 2008;18:3745-58.

[2] Arruebo M, Galán M, Navascués N, Téllez C, Marquina C, Ibarra MR, et al. Development of magnetic nanostructured silica-based materials as potential vectors for drug-delivery applications. *Chem Mater.* 2006;18:1911-9.

[3] Xiao K, Luo J, Li Y, Lee JS, Fung G, Lam KS. PEG-oligocholic acid telodendrimer micelles for the targeted delivery of doxorubicin to B-cell lymphoma. *J Control Release.* 2011;155:272-81.

[4] Li Y, Lin T-y, Luo Y, Liu Q, Xiao W, Guo W, et al. A smart and versatile theranostic nanomedicine platform based on nanoporphyrin. *Nat Commun.* 2014;5.

[5] Shi J, Choi JL, Chou B, Johnson RN, Schellinger JG, Pun SH. Effect of Polyplex Morphology on Cellular Uptake, Intracellular Trafficking, and Transgene Expression. *ACS Nano.* 2013;7:10612-20.

[6] Sugano M, Egilmez NK, Yokota SJ, Chen F-A, Harding J, Huang SK, et al. Antibody targeting of doxorubicin-loaded liposomes suppresses the growth and metastatic spread of established human lung tumor xenografts in severe combined immunodeficient mice. *Cancer Res.* 2000;60:6942-9.

[7] Chen K-J, Liang H-F, Chen H-L, Wang Y, Cheng P-Y, Liu H-L, et al. A thermoresponsive bubble-generating liposomal system for triggering localized extracellular drug delivery. *ACS Nano.* 2012;7:438-46.

[8] Sun X, Liu Z, Welsher K, Robinson JT, Goodwin A, Zaric S, et al. Nano-graphene oxide for cellular imaging and drug delivery. *Nano Res.* 2008;1:203-12.

[9] Dembereldorj U, Choi SY, Ganbold EO, Song NW, Kim D, Choo J, et al. Gold Nanorod-Assembled PEGylated Graphene-Oxide Nanocomposites for Photothermal Cancer Therapy. *Photochem Photobiol.* 2014;90:659-66.

[10] Wen S, Liu H, Cai H, Shen M, Shi X. Targeted and pH-Responsive Delivery of Doxorubicin to Cancer Cells Using Multifunctional Dendrimer-Modified Multi-Walled Carbon Nanotubes. *Adv Healthc Mater.* 2013;2:1267-76.

[11] Shah BP, Pasquale N, De G, Tan T, Ma J, Lee K-B. Core-Shell Nanoparticle-Based Peptide Therapeutics and Combined Hyperthermia for Enhanced Cancer Cell Apoptosis.

ACS Nano. 2014.

[12] Arruebo M, Fernández-Pacheco R, Ibarra MR, Santamaría J. Magnetic nanoparticles for drug delivery. *Nano today*. 2007;2:22-32.

[13] Xia Y, Li W, Cobley CM, Chen J, Xia X, Zhang Q, et al. Gold nanocages: from synthesis to theranostic applications. *Acc Chem Res*. 2011;44:914-24.

[14] Huang XH, El-Sayed IH, Qian W, El-Sayed MA. Cancer cell imaging and photothermal therapy in the near-infrared region by using gold nanorods. *J Am Chem Soc*. 2006;128:2115-20.

[15] von Maltzahn G, Park J-H, Agrawal A, Bandaru NK, Das SK, Sailor MJ, et al. Computationally guided photothermal tumor therapy using long-circulating gold nanorod antennas. *Cancer Res*. 2009;69:3892-900.

[16] Yuan H, Fales AM, Vo-Dinh T. TAT peptide-functionalized gold nanostars: enhanced intracellular delivery and efficient NIR photothermal therapy using ultralow irradiance. *J Am Chem Soc*. 2012;134:11358-61.

[17] Nergiz SZ, Gandra N, Tadepalli S, Singamaneni S. Multifunctional Hybrid Nanopatches of Graphene oxide and Gold Nanostars for Ultra-efficient Photothermal

Cancer therapy. *ACS Appl Mater Interfaces*. 2014.

[18] Ayala-Orozco C, Urban C, Knight MW, Urban AS, Neumann O, Bishnoi SW, et al. Au Nanomatryoshkas as Efficient Near-Infrared Photothermal Transducers for Cancer Treatment: Benchmarking against Nanoshells. *ACS Nano*. 2014.

[19] Jang H, Kim YK, Huh H, Min DH. Facile Synthesis and Intraparticle Self-Catalytic Oxidation of Dextran-Coated Hollow Au-Ag Nanoshell and Its Application for Chemo-Thermotherapy. *ACS Nano*. 2014;8:467-75.

[20] Park H, Yang J, Seo S, Kim K, Suh J, Kim D, et al. Multifunctional nanoparticles for photothermally controlled drug delivery and magnetic resonance imaging enhancement. *Small*. 2008;4:192-6.

[21] Hwang S, Nam J, Jung S, Song J, Doh H, Kim S. Gold nanoparticle-mediated photothermal therapy: current status and future perspective. *Nanomedicine*. 2014;9:2003-22.

[22] Song J, Fang Z, Wang C, Zhou J, Duan B, Pu L, et al. Photolabile plasmonic vesicles assembled from amphiphilic gold nanoparticles for remote-controlled traceable drug delivery. *Nanoscale*. 2013;5:5816-24.

[23] Kim H, Lee D, Kim J, Kim T-i, Kim WJ. Photothermally triggered cytosolic drug delivery via endosome disruption using a functionalized reduced graphene oxide. *ACS Nano*. 2013;7:6735-46.

[24] Wang F, Wang Y-C, Dou S, Xiong M-H, Sun T-M, Wang J. Doxorubicin-tethered responsive gold nanoparticles facilitate intracellular drug delivery for overcoming multidrug resistance in cancer cells. *ACS Nano.* 2011;5:3679-92.

[25] Cho K, Wang X, Nie S, Shin DM. Therapeutic nanoparticles for drug delivery in cancer. *Clin Cancer Res.* 2008;14:1310-6.

[26] Choi G, Kwon O-J, Oh Y, Yun C-O, Choy J-H. Inorganic Nanovehicle Targets Tumor in an Orthotopic Breast Cancer Model. *Sci Rep.* 2014;4.

[27] Sun Y, Mayers BT, Xia Y. Template-engaged replacement reaction: a one-step approach to the large-scale synthesis of metal nanostructures with hollow interiors. *Nano Lett.* 2002;2:481-5.

[28] You J, Zhang G, Li C. Exceptionally high payload of doxorubicin in hollow gold nanospheres for near-infrared light-triggered drug release. *ACS Nano.* 2010;4:1033-41.

[29] Smith DK, Miller NR, Korgel BA. Iodide in CTAB prevents gold nanorod formation.

Langmuir. 2009;25:9518-24.

[30] Paez JG, Jänne PA, Lee JC, Tracy S, Greulich H, Gabriel S, et al. EGFR mutations in lung cancer: correlation with clinical response to gefitinib therapy. *Science.* 2004;304:1497-500.

[31] Yang LL, Mao H, Wang YA, Cao ZH, Peng XH, Wang XX, et al. Single Chain Epidermal Growth Factor Receptor Antibody Conjugated Nanoparticles for in vivo Tumor Targeting and Imaging. *Small.* 2009;5:235-43.

[32] Creixell M, Bohórquez AC, Torres-Lugo M, Rinaldi C. EGFR-targeted magnetic nanoparticle heaters kill cancer cells without a perceptible temperature rise. *ACS Nano.* 2011;5:7124-9.

[33] Melancon MP, Lu W, Yang Z, Zhang R, Cheng Z, Elliot AM, et al. In vitro and in vivo targeting of hollow gold nanoshells directed at epidermal growth factor receptor for photothermal ablation therapy. *Mol Cancer Ther.* 2008;7:1730-9.

[34] Harush-Frenkel O, Debotton N, Benita S, Altschuler Y. Targeting of nanoparticles to the clathrin-mediated endocytic pathway. *Biochem Biophys Res Commun.* 2007;353:26-32.

[35] Kim J-S, Yoon T-J, Yu K-N, Noh MS, Woo M, Kim B-G, et al. Cellular uptake of magnetic nanoparticle is mediated through energy-dependent endocytosis in A549 cells. *J Vet Sci*. 2006;7:321-6.

[36] Kang H, Yang J-K, Noh MS, Jo A, Jeong S, Lee M, et al. One-Step Synthesis of Silver Nanoshell with Bumps for Highly Sensitive Near-IR SERS Nanoprobes. *J Mater Chem B*. 2014;2:4415-21.

[37] Yang J-K, Kang H, Lee H, Jo A, Jeong S, Jeon S-J, et al. Single-Step and Rapid Growth of Silver Nanoshells as SERS-Active Nanostructures for Label-Free Detection of Pesticides. *ACS Applied Materials & Interfaces*. 2014;6:12541-9.

[38] Loo C, Lowery A, Halas N, West J, Drezek R. Immunotargeted nanoshells for integrated cancer imaging and therapy. *Nano Lett*. 2005;5:709-11.

[39] Jain PK, Lee KS, El-Sayed IH, El-Sayed MA. Calculated absorption and scattering properties of gold nanoparticles of different size, shape, and composition: applications in biological imaging and biomedicine. *J Phys Chem B*. 2006;110:7238-48.

[40] Liao HW, Hafner JH. Gold nanorod bioconjugates. *Chem Mater*. 2005;17:4636-41.

[41] Connor EE, Mwamuka J, Gole A, Murphy CJ, Wyatt MD. Gold nanoparticles are

taken up by human cells but do not cause acute cytotoxicity. *Small.* 2005;1:325-7.

[42] Wang S, Lu W, Tovmachenko O, Rai US, Yu H, Ray PC. Challenge in understanding size and shape dependent toxicity of gold nanomaterials in human skin keratinocytes. *Chem Phys Lett.* 2008;463:145-9.

[43] Yokoyama T, Tam J, Kuroda S, Scott AW, Aaron J, Larson T, et al. EGFR-targeted hybrid plasmonic magnetic nanoparticles synergistically induce autophagy and apoptosis in non-small cell lung cancer cells. *PLoS One.* 2011;6:e25507.

[44] Xie M, Shi H, Li Z, Shen H, Ma K, Li B, et al. A multifunctional mesoporous silica nanocomposite for targeted delivery, controlled release of doxorubicin and bioimaging. *Colloids Surf B Biointerfaces.* 2013;110:138-47.

[45] Engelman JA, Jänne PA, Mermel C, Pearlberg J, Mukohara T, Fleet C, et al. ErbB-3 mediates phosphoinositide 3-kinase activity in gefitinib-sensitive non-small cell lung cancer cell lines. *Proc Natl Acad Sci U S A.* 2005;102:3788-93.

[46] Ono M, Hirata A, Kometani T, Miyagawa M, Ueda S-i, Kinoshita H, et al. Sensitivity to gefitinib (Iressa, ZD1839) in non-small cell lung cancer cell lines correlates with dependence on the epidermal growth factor (EGF) receptor/extracellular signal-regulated kinase 1/2 and EGF receptor/Akt pathway for proliferation. *Mol Cancer Ther.*

2004;3:465-72.

[47] Kim D, Jeong YY, Jon S. A drug-loaded aptamer− gold nanoparticle bioconjugate for combined CT imaging and therapy of prostate cancer. *ACS Nano*. 2010;4:3689-96.

[48] Gillies ER, Fréchet JM. pH-responsive copolymer assemblies for controlled release of doxorubicin. *Bioconjug Chem*. 2005;16:361-8.

[49] Goodman AM, Cao Y, Urban C, Neumann O, Ayala-Orozco C, Knight MW, et al. The Surprising in Vivo Instability of Near-IR-Absorbing Hollow Au–Ag Nanoshells. *ACS Nano*. 2014;8:3222-31.

[50] Hillaireau H, Couvreur P. Nanocarriers' entry into the cell: relevance to drug delivery. *Cell Mol Life Sci.* 2009;66:2873-96.

[51] Sahay G, Alakhova DY, Kabanov AV. Endocytosis of nanomedicines. *J Control Release.* 2010;145:182-95.

[52] Zaki NM, Tirelli N. Gateways for the intracellular access of nanocarriers: a review of receptor-mediated endocytosis mechanisms and of strategies in receptor targeting. *Expert Opin Drug Deliv.* 2010;7:895-913.

[53] Zhang X, Meng L, Lu Q, Fei Z, Dyson PJ. Targeted delivery and controlled release of doxorubicin to cancer cells using modified single wall carbon nanotubes. *Biomaterials*. 2009;30:6041-7.

[54] Yang X, Liu Z, Li Z, Pu F, Ren J, Qu X. Near-Infrared-Controlled, Targeted Hydrophobic Drug-Delivery System for Synergistic Cancer Therapy. *Chemistry*. 2013;19:10388-94.

[55] McNeeley KM, Karathanasis E, Annapragada AV, Bellamkonda RV. Masking and triggered unmasking of targeting ligands on nanocarriers to improve drug delivery to brain tumors. *Biomaterials*. 2009;30:3986-95.

국문 논문 초록

금/은 빈 공간 나노쉘의 폐암 세포 표면 축적을 이용한 특정 세포 탐지 기능성 근적외선 유도약물 방출 및 광열 치료 효과

노 미 숙

융합과학기술대학원 융합과학부 나노융합전공

다양한 나노물질과 나노구조들은 나노스케일의 고유한 특징 때문에 의생물학적 적용에 유망한 후보물질로 기대를 받고 있다. 높은 표면적, 작은 크기, 양자구속효과, 자성 및 광학 효과들을 나노입자에 도입하여 진단과 치료 기술을 개발할 수 있다. 하나의 나노사이즈의 장치에 다양한 기능을 통합하는 것은 최근 각광 받는 분야이다.

약물전달기술에 적용하는 기술로, 나노사이즈의 장치에 근적외선에서 빛의 산란을 활용할 수 있는 금속물질을 코팅할 수 있다. 이 때 근적외선 레이저로 자극을 주면, 금속나노물질의 광열적 효과로 암 세포에 적용 시 지역적인 온도를 올려주고, 나노쉘 구조 중 다공성을 가진 형태는 약물을 그 안에 보관하고 있다가 특정 조건에 의해 약물 방출을 유도하는 것이 가능하다.

본 논문에서는 금과 은이 코팅된 빈 공간을 가진 나노 쉘(AuHNS)을 개발하여 효과적으로 특정 암세포 표면에 탐지할 수 있으며, 광 치료의 효과 및 근적외선 레이저 적용 시 약물을 방출할 수 있는 다양한 기능을 가진 약물전달물질을 개발하고자 하였다. 은나노쉘(AgNS)로부터 내부에 빈 공간을 만들기 위해서는 갈바닉교환반응이 이용되며, 금/은 코팅의 빈 공간을 가진 나노쉘의 구조로 변화된다. 상피 성장인자 수용기 (EGFR)에 대한 항체를 페길레이션된 AuHNS 에 결합시키고, 항생제인 독소루비신을 처리하여 빈 공간 내부에 항생제가 들어갈 수 있도록 하였으며, 상피 성장인자 수용기가 표면에 많은 폐암에 선택적 치료로 적용하고자 하였다. 금 나노로드 형태의 나노물질은 기존 광열치료 효과에 많이 활용되었으며, 이러한 단독 나노 디바이스는 금 나노로드 형태의 나노물질과의 비교를 위하여 같은 근적외선 레이저의 세기로 조사하였을 때, 유사한 광 치료 효과를 가지는 것으로 확인되었다. 또한, 폐암세포인 A549 를 활용하여 이러한 복합체(AuHNS-EGFR-DOX)가 특이적으로 세포를 탐지하는 능력이 있다는 것을 빛 산란 이미지로 증명하였고, 독소루비신의 방출이 pH 와 근적외선 레이저의 조사에 따라 변화되는 것을 확인하였다. 따라서, 다양한 기능이 함축된 복합체는 탐지 능력을 가진 폐암세포에서의 광열 치료와 근적외선 레이저의 조사에 의한 빠른 독소루비신 방출이 가능하도록 유도하였으며, 가장 효과적인 복합체의 활용을 위하여 두 가지 약물 전달 방법을 비교하였다. 첫 번째는 수용체를 통한 내포작용 그리고 두 번째는 세포표면의 표적 항원에 탐지하는 방법을 이용한 약물 방출인데, 세포 표면 위에 상피 성장 인자 수용체에 결합하여 이 복합체가 축적되면, 내포작용에 의한 치료효과보다 더 뛰어난 효과를 가져오는 것을 확인할 수 있었다. 따라서, 암 세포 표면에 탐지기능을 포함한 복합체를 축적시켜 근적외선

조사에 의한 약물 방출 효과를 증대하는 최적의 방법을 고안하여, 폐암의 치료효과를 높이고자 하였다. 이러한 근적외선 탐지를 활용한 선택적 약물전달 방법을 연구하여 앞으로 의학기술에 적용할 때, 높은 성능을 가진 항암 약물 전달 치료 시스템으로 진전될 수 있을 것으로 기대된다.